Analytical framework for predicting stiffness in single wooden dowel timber-to-timber connections

Structures 91 (2026) 112538

Contents lists available at ScienceDirect

Structures

journal homepage: www.elsevier.com/locate/structures

Analytical framework for predicting stiffness in single wooden dowel timber-to-timber connections

Inayat Ullah Khan [a,*], Mahbube Subhani [b], Kazem Ghabraie [a], Mahmud Ashraf [a]

[a] School of Engineering, Deakin University, Waurn Ponds, Geelong, VIC 3216, Australia

[b] Division of Structural Engineering, Department of Architecture and Civil Engineering, Chalmers University of Technology, Sweden

ARTICLE INFO

Keywords:
Wooden dowels
single dowel connections
joint stiffness
theoretical models

ABSTRACT

Engineered wood products (EWPs) connected with wooden dowels, commonly referred to as dowel-laminated timber (DLT), are increasingly adopted due to their recyclability, on site adaptability, absence of synthetic adhesives, rapid assembly, and design flexibility. The structural efficiency of DLT systems is governed by joint stiffness, which serves as a key input for the gamma and the shear analogy method used to evaluate the effective bending stiffness of DLT beams and panels. In practice, this stiffness is derived from tests on single wooden dowel timber-to-timber connections (WDTCs). Despite their importance, a comprehensive evaluation of existing theoretical stiffness models, alternative formulations, and their predictive accuracy for WDTCs remains lacking. Current Eurocode 5 stiffness provisions are not directly applicable to WDTCs because their governing failure mechanisms differ fundamentally from those of metal fastener timber-to-timber connections (MFTCs), involving coupled dowel embedment, bending, shear, and timber deformation. Similarly, the Timber Frame Engineering Council (TFEC) standard addresses the strength of pegged mortise and tenon joints but provides no guidance on stiffness. Unlike metal fasteners, wooden dowels deform significantly; therefore, the influence of key geometric and material parameters on WDTC stiffness differs from that of MFTCs and remains insufficiently quantified. Moreover, empirical equations for predicting WDTC stiffness are scarce in the literature. To address these gaps, this study refines, validates, and proposes several mechanics-based stiffness models for WDTCs, including beam on elastic foundation (BEF), spring in series (S-S), rigid rotation with friction (RRF), embedment stiffness, simply supported dowel (SSB) models, and selected codified formulations. Statistical analyses, including analysis of variance and best subset regression, are conducted to quantify parameter influence and to develop new empirical input model. All prediction models are validated against a comprehensive dataset compiled from the literature, and a new embedment-based stiffness formulation is introduced. The BEF, RRF and embedment stiffness approaches achieve stiffness predictions with maximum deviations below 20 % across the dataset. Finally, a practical and validated design framework for predicting WDTC stiffness is proposed.

1. Introduction

Dowel-laminated timber (DLT), in which multiple layers of timber are connected using wooden dowels, has gained increasing attention from both researchers and manufacturers. DLT supports computer numerical control (CNC) manufacturing, enables ease of recycling due to the absence of metal fasteners, allows for on-site modifications, and ensures material compatibility [1]. Unlike glued laminated products, DLT avoids problems associated with adhesive bonding in dense timber and is free from toxic or wasteful adhesives [2,3]. A notable initiative in this field is the Adhesive-Free Timber Buildings (AFTB) project under Interreg North-West Europe (NWE), which focused on compressed wooden DLT [4]. StructureCraft, a North American company, has implemented more than 150 projects utilizing DLT of various typologies

List of Abbreviations: DLT, Dowel-laminated timber; CNC, Computer numerical control; EWPs, Engineered wood products; WDTCs, Wooden dowel timber-to-timber connections; MFTCs, Metal fastener timber-to-timber connections; BEF, Beam-on-elastic-foundation; DS, Double shear; RRF, Rigid rotation with friction; MC, Moisture content; SD, Standard deviation; AFTB, Adhesive-Free Timber Buildings; NWE, North-West Europe; CLT, Cross-laminated timber; NDS, National Design Specifications; EC5, Eurocode 5; S-S, Spring in series; SS, Single shear; TFEC, Timber Frame Engineering Council; ANOVA, Analysis of variance; SSB, Simply supported beam.

* Corresponding author.
E-mail address: inayat.khan@deakin.edu.au (I.U. Khan).

https://doi.org/10.1016/j.istruc.2026.112538
Received 24 February 2026; Received in revised form 13 May 2026; Accepted 29 June 2026
Available online 2 July 2026

since 2017 [5]. Despite these advantages and its growing adoption, DLT remains a relatively new product with limited research, and comprehensive guidelines for evaluating its structural performance are still lacking [6]. A critical component is the interlayer connection. DLT layers are connected using wooden dowels to transfer forces between layers; these joints are referred to as DLT connections or wooden dowel timber-to-timber connections (WDTCs). Overall, the structural performance of DLT systems is governed by the efficiency of these connections [7,8]. For DLT bending elements, this efficiency depends directly on joint stiffness, which is a key input to the gamma method and the shear analogy method for evaluating the effective bending stiffness of beams and panels [9]. Consequently, reliable prediction of WDTC stiffness is essential.

Empirical and mechanics-based models are widely used in timber engineering to predict connection performance without the need for extensive experimental testing. For WDTCs, accurate stiffness prediction requires a clear understanding of the underlying deformation mechanisms, which can subsequently be translated into mathematical formulations. However, currently available stiffness models for WDTCs remain limited in the literature. Eurocode 5 (EC5) [10] provides stiffness models for MFTCs, which are not directly applicable to WDTCs. MFTCs typically fail by dowel bending or timber embedment, whereas WDTCs exhibit more complex, interacting mechanisms. The principal modes are dowel shear, dowel bending, dowel embedment, and timber embedment [11,12]; in practice these rarely occur alone. Mixed forms such as simultaneous embedment, bending, and shear are common and are grouped as Mode V [11,13]. Failure Mode V refers to the mixed-mode failure mechanism that occurs in wooden dowels. It involves multiple longitudinal shear fractures in the dowel, kinked fibre bundles from bending, and compression perpendicular to the grain in both dowel and timber, producing a ductile response. Because the mechanical properties of the dowel and the surrounding timber are comparable, deformation develops in both materials, and joint stiffness depends on their combined behaviour [14,15]. Therefore, one of the key challenges in predicting the stiffness of WDTCs is accounting for these multiple interacting deformations.

The key parameters affecting joint stiffness in WDTCs have been examined in only a limited number of studies, and their influence remains incompletely understood. Existing investigations are largely experimental in nature [16,17]. Fu et al. [18] evaluated the effects of main and side member thickness in double shear (DS) connections. El Houjeyri et al. [19] studied the influence of dowel material (oak and compressed spruce) in DS joints of spruce and oak. Li and Zhou [20] tested bamboo DS connections with dowel diameters of 6, 8, 10, and 12 mm. Frontini et al. [21] investigated the effects of dowel diameter, dowel shape, and timber grain orientation on stiffness. Vilguts et al. [22] examined single shear (SS) joints with varying dowel diameters and species. Sandberg et al. [11] analysed the impact of side and main member thickness on stiffness. Zhang et al. [23] explored the effect of prestressing in DS joints, and Ceraldi et al. [24,25] tested chestnut and fir joints to assess the role of timber density. Despite these contributions, there is still no comprehensive study that critically synthesises the parameters governing WDTC stiffness, nor one that systematically evaluates theoretical models for stiffness prediction; most work remains focused on experimental results. However, integrating these experimental findings can provide a robust database for validating newly proposed analytical models or calibrating existing equations developed for MFTCs.

Experimental testing of timber connections is costly and labour intensive, while designers prefer simple and reliable formulations for practical design. Only a limited number of studies have proposed theoretical models for predicting the stiffness of WDTCs. Fukuyama et al. [16,17] developed mechanics-based joint stiffness models; however, their applicability to a wide range of WDTC configurations, including different timber species, dowel diameters, and member thicknesses, has not been comprehensively validated. The authors [26] have previously conducted experimental studies on radiata pine and spotted gum connections using Tasmanian oak dowels and validated their stiffness using mechanics-based models. Nevertheless, extending these models to a broader range of WDTC configurations remains an important research gap. Vilguts et al. [22] developed an empirical stiffness model for wooden dowel connections in cross-laminated timber (CLT), based on tests of CLT manufactured from douglas fir, grand fir, western hemlock, and spruce pine fir, using red oak and birch dowels with diameters of 19.0 mm and 25.4 mm. The model was limited to CLT connections and incorporated the dowel and timber properties through their specific gravities. However, experimental studies [15,18] have shown that joint stiffness is also influenced by the thicknesses of the side and main members, an effect not captured by this model. Overall, existing regression-based models remain limited, highlighting a significant research gap in the development, refinement, and validation of both empirical and mechanics-based stiffness models for wooden dowel connections.

Building on these gaps, limited understanding of parameters governing WDTC stiffness, few mechanics-based models with broad applicability, scarce regression models using wide ranging datasets, and the absence of a design framework, this study addresses the need for a comprehensive stiffness assessment of WDTCs. The purpose is to investigate the mechanical performance of WDTCs in terms of stiffness using theoretical approaches. The overall aim is to refine, validate, and propose models for predicting the stiffness of single wooden dowel connections, and to present a design framework for their application. The specific objectives are: (a) to compile and analyse literature data to identify parameters that influence WDTC stiffness; (b) to evaluate existing theoretical models, develop new models for stiffness prediction, and assess their deviations against published dataset; (c) to apply best subset regression and ANOVA to determine the statistical significance of governing parameters and to derive new empirical regression model; and (d) to propose a practical design framework to predict the stiffness of WDTC.

1.1. Definitions and empirical formulation

In this paper, the terms WDTCs, wooden dowel connections, and DLT connections are used interchangeably. Wooden dowel denotes the connector element, whereas “timber” refers to the members (side or main) in WDTCs. At 12% moisture content (MC), the bending elastic modulus E for clear, straight grained wood, as reported in the Wood Handbook [27], is expressed in MPa and given by Eq. 1 as a function of the specific gravity G. This empirical formulation is referenced throughout this study.

$$E = \begin{cases} 20300G^{0.83} & \textit{softwoods} \\ 16500G^{0.70} & \textit{hardwoods} \end{cases} \tag{1}$$

EN 384 [28] specifies that the shear modulus (G) can be estimated from the E using the relationship G=E/16.

Existing studies on WDTCs are summarized in Table 1, and the terms used in the table are illustrated in Fig. 1. The mean values presented in the table also include a column for the number of tests (n), resulting in a total of 644 tests. In the table, ρ_d and ρ_t represent the densities of the dowel and timber at 12% MC, respectively. Specific gravity values, required anywhere in this paper, are derived from these densities according to ASTM D2395–17 [29]. P_y, $P_{\max}$, and K denote the yield load, maximum load capacity, and joint stiffness of the WDTCs, respectively. The joint stiffness reported in this paper is determined in the linear elastic range, following the procedures in ASTM D5652–21 [30] and ISO/TR 21141 [31]. The dowel diameter is indicated as D or d. All subsequent discussion, including theoretical model's predictions, is based entirely on the data in Table 1.

Table 1
Summary of studies on WDTCs from the literature.

Studies	Dowel Material	ρ_d	D	Middle & side members	n	ρ_t	L	w	t_s or t_1	t_m or t_2	Load direction (single / double shear)	P_y	P_{max}	K	Failure modes/Comments
		kg/m3	mm			kg/m3	mm	mm	mm	mm		kN	kN	kN/mm	
Fu et al. [18]	Beech (Fagus) Dowel 3-point bending (L = 240 mm) P_y = 0.586 kN and P_{max} = 0.834 kN.	711	16	Larch LVL	5	530	300	140	20	20	Along grain, DS	8.15	9.52	5.43	Three plastic hinges, Lamella inclination, Hole extrusion
		711	16		5	530	300	140	20	30		7.38	9.98	5.80	
		711	16		5	530	300	140	20	40		7.89	9.95	5.37	
		711	16		5	530	300	140	20	20	Perp to grain, DS	7.13	8.50	3.56	Dowel shear failure, Two plastic hinges
		711	16		5	530	300	140	40	40	Along grain, DS	10.12	15.34	6.93	
		711	16		5	530	300	140	60	60		9.76	14.91	6.57	
El-Houjeyri et al. [19]	Spruce Compressed dowels	1133	16	Spruce	5	420	250	80	42	42	Along grain, DS		12.97	3.65	Shear and tension failure of dowels, Embedment failure of timber Note: The maximum load capacity joints was approximately estimated from their experimental force–deformation curves.
	Uncompressed Oak	620	16	Spruce	4	420	250	80	42	42			5.38		
	Spruce CW dowels	1133	16	Oak	4	620	250	80	42	42			20.14	7.06	
	Uncompressed Oak	620	16	Oak	5	620	250	80	42	42			6.5		
Tétreault et al. [32]	Compressed Spruce dowel	1158	16	Glued laminated spruce-pine-fir timber	5	560	250	80	50	50	Along grain, DS		16	6	Dowel shearing, Timber embedment
Li and Zhou [20]	Phyllostachys pubescens (Moso bamboo) China, Laminated bamboo lumber (LBL)	1300	6	LBL (Moso bamboo) in China	5	1300	150	80	30	60	Load along grain, DS		1.87	-	Dowel bearing, hole embedment, and the yielding with secondary bending failure of dowel.
		1300	8		5	1300	150	80	30	60			3.32	-	
		1300	10		5	1300	150	80	30	60			4.07	-	
		1300	12		5	1300	150	80	30	60			5.86	-	
Frontini et al. [21]	Pine (Norway)	427	10	Pine (Norway)	6	494.1	210	60	30	30	Along grain, DS		3.85	2.05	Round dowel (CYC)
		427	10		6	494.1	210	60	30	30			4.44	2.93	Octagonal constant cross-section (CYT)
		427	20		6	494.1	420	120	30	30			10.33	3.53	CYC
		427	20		6	494.1	420	120	30	30			9.75	4.16	CYT
		427	10		5	463.2	210	60	30	30	Along grain, SS		1.79	1.09	CYC
		427	10		5	463.2	210	60	30	30			1.9	1.55	CYT
		427	10		5	463.2	210	60	30	30			1.96	1.44	Conical (CON) pegs – square cross-sections
		427	15		5	463.2	315	90	30	30			2.38	2.02	CYC
		427	15		5	463.2	315	90	30	30			2.61	2.47	CYT
		427	15		5	463.2	315	90	30	30			2.9	3.08	Conical (CON-S) pegs – square cross-sections
		427	20		5	463.2	420	120	30	30			3.78	2.07	CYC
		427	20		5	463.2	420	120	30	30			4.32	3.58	CYT
		427	20		5	463.2	420	120	30	30			4.19	3.37	Conical (CON-O) pegs – octagonal cross-sections
		427	10	Pine (Norway) central member width = 20d, side members = 6d.	5	438.1	100	60	30	30	Central member perpendicular to the grain, side members parallel to the grain, DS		3.28	2.23	CYC
		427	10		5	438.1	100	60	30	30			3.88	2.46	CYT
		427	20		5	438.1	200	120	30	30			8.7	3.15	CYC
		427	20		5	438.1	200	120	30	30			8.48	3.27	CYT
		427	10	Pine (Norway) left member width = 6d, right member = 20d.	6	448.4	100	60	30	30	Left member (1) parallel to the grain, right member (2) perpendicular to the grain, SS		1.69	0.65	CYC
		427	10		6	448.4	100	60	30	30			1.85	0.83	CYT
		427	10		6	448.4	100	60	30	30			1.88	0.66	CON
		427	15		6	448.4	150	90	30	30			2.86	0.82	CYC
		427	15		6	448.4	150	90	30	30			2.88	1.1	CYT
		427	15		6	448.4	150	90	30	30			3	0.62	CON
		427	20		6	448.4	200	120	30	30			3.84	1.2	CYC
		427	20		6	448.4	200	120	30	30			4.13	1.84	CYT

(*continued on next page*)

Table 1 (*continued*)

Studies	Dowel Material	ρ_d	D	Middle & side members	n	ρ_t	L	w	t_s or t_1	t_m or t_2	Load direction (single / double shear)	P_y	P_{max}	K	Failure modes/Comments
		427	20		6	448.4	200	120	30	30			3.79	0.95	CON
		427	10	Pine (Norway) left member width = 6d, right member = 20d.	4	421.6	100	60	30	30	Left member (1) parallel to the grain, right member (2) perpendicular to the grain, with a gap between members, SS		1.12	0.11	CYC
		427	10		4	421.6	100	60	30	30			1.14	0.15	CYT
		427	10		4	421.6	100	60	30	30			1.21	0.18	CON
		427	15		4	421.6	150	90	30	30			1.88	0.29	CYC
		427	15		4	421.6	150	90	30	30			2.09	0.27	CYT
		427	15		4	421.6	150	90	30	30			1.76	0.22	CON
		427	20		4	421.6	200	120	30	30			3.34	0.3	CYC
		427	20		4	421.6	200	120	30	30			3.45	0.54	CYT
		427	20		4	421.6	200	120	30	30			3.04	0.24	CON
Vilguts et al. [22]	Red Oak (RO)	664	25.4	Douglas-Fir larch (DF)	12	503.4	380	140	90	90	The CLT specimens were cut from 3-ply thick lamellas made of the given timber (total thickness 90 mm). The CLT plates were bonded using polyurethane reactive adhesive (PUR) under a manufacturing pressure of 0.7 MPa (100 psi), SS	10.3		5.2	Longitudinal shear failure followed by combination of tension and further shear with some dowel bearing
		664	25.4	Grand-Fir (GF)	12	398.1	380	140	90	90		10.32		5.18	
		664	25.4	Western-Hemlock (WH)	12	451.7	380	140	90	90		9.73		4.76	
		664	25.4	Spruce-Pine-Fir (SPF)	8	457.3	380	140	90	90		9.87		4.89	
	Yellow Birch (B)	614.9	25.4	DF	12	503.4	380	140	90	90		8.41		3.69	
		614.9	25.4	GF	12	398.1	380	140	90	90		8.48		3.66	
		614.9	25.4	WH	12	451.7	380	140	90	90		8.76		3.52	
		614.9	25.4	SPF	8	457.3	380	140	90	90		9.47		3.74	
	RO	663.2	19	DF	8	503.4	340	140	90	90		5.69		3.94	
		663.2	19	GF	8	398.1	340	140	90	90		5.91		3.7	
		663.2	19	WH	8	451.7	340	140	90	90		6.01		3.43	
		663.2	19	SPF	8	457.3	340	140	90	90		6.05		3.28	
	B	617.9	19	DF	8	503.4	340	140	90	90		6.41		3.07	
		617.9	19	GF	8	398.1	340	140	90	90		5.5		2.93	
		617.9	19	WH	8	451.7	340	140	90	90		5.78		2.59	
		617.9	19	SPF	8	457.3	340	140	90	90		5.56		2.66	
Ceraldi et al. [24,25]	Ash	652	30	Chestnut (Castanea sativa) 32.8 MPa compression strength	3	523	300	200	60	90	Along grain, DS	24.7	38.9	8.7	Combination of peg shearing, peg bending, and peg dowel-bearing yielding named "effective peg shear (IV/V)
	Ash	652	30	Fir (Abies alba) 39.2 MPa compression strength	3	472	300	200	60	90	Along grain, DS	21.6	33.9	7.62	
Bouhala et al. [33]	Compressed Scots Pine (Pinus sylvestris)	1200	10	Scots Pine (Pinus sylvestris	3	550	250	80	30	30	Along grain, DS		7.5	3.75	Load capacity and stiffness values are estimated from the force–deformation curves.
Bruzzone et al. [15]	guatambú (Balfourodendron riedelianum)	850	20	Pine (Pinus elliotti)	10	399	248	138	50	50	Main member parallel and side members Perpendicular to grain. The side members have a width three times that of the main member and a length equal to their width. DS		14.09	3.03	Combined failure in bending and shear Failure mode (IV, EN 1995–1–1).
	Eucalyptus grandis	475	20	Pine (Pinus elliotti)	8	399	248	138	50	50			7.06	1.79	
	Red gum (Eucalyptus tereticornis)	700	18	Eucalyptus grandis	7	475	248	89	36	36			7.35	2.78	
	Red gum (Eucalyptus tereticornis)	700	15	Eucalyptus grandis	9	475	248	89	36	36			4.66	1.27	
Burnett et al. [14]	Northern red oak	788	25.4	Eastern white pine	9	410	533.4	190.5	44.45	44.45	Main member parallel and side members Perpendicular to grain, DS	13.50	14.56	2.39	Ductile peg failure. Values converted from lb to kN. Specific gravities were converted to densities.
	Northern red oak	788	25.4	Douglas Fir	9	530	533.4	190.5	44.45	44.45		15.88	15.97	3.74	
	Northern red oak	788	25.4	Northern red oak	10	750	533.4	190.5	44.45	44.45		15.56	16.05	3.23	

(*continued on next page*)

Table 1 (*continued*)

Studies	Dowel Material	ρ_d	D	Middle & side members	n	ρ_t	L	w	t_s or t_1	t_m or t_2	Load direction (single / double shear)	P_y	P_{max}	K	Failure modes/Comments
Minari et al. [34]	Peltogyne spp. (Purpleheart or violet wood)	800	19	Pinus taeda and Pinus elliottii	11	550	210	90	38	38	Along grain, DS		15.29	8	Bending of the dowels, Embedding in the wood pieces. Density values taken from literature.
Sandberg et al. [11]	Northern red oak (Quercus rubra)	719	25.4	Eastern white pine (Pinus strobus)	9	388	152.4	152.4	25.4	50.8	Parallel to grain of tenon, perpendicular to grain of mortise, DS	15.77		6.04	Failure mode V AND dowel embedment
		719	25.4		9	388	152.4	152.4	25.4	50.8	Perpendicular to grain of tenon, parallel to grain of mortise, DS	15.28		5.76	
		719	25.4		9	388	152.4	152.4	50.8	50.8	Parallel to grain of tenon, perpendicular to grain of mortise, DS	15.85		6.29	
		719	25.4		9	388	152.4	152.4	50.8	50.8	Perpendicular to grain of tenon, parallel to grain of mortise, DS	16.47		5.74	
		719	25.4	Sugar maple (Acer saccharum).	9	729	152.4	152.4	25.4	50.8	Parallel to grain of tenon, perpendicular to grain of mortise, DS	17.87		8.17	
		719	25.4		9	729	152.4	152.4	25.4	50.8	Perpendicular to grain of tenon, perpendicular to grain of mortise, DS	18.7		8.93	
		719	25.4		9	729	152.4	152.4	50.8	50.8	Parallel to grain of tenon, perpendicular to grain of mortise, DS	18.26		8.72	
		719	25.4		9	729	152.4	152.4	50.8	50.8	Perpendicular to grain of tenon, perpendicular to grain of mortise, DS	17.06		7.85	
Teodorescu et al. [35]	Massaranduba F_{max}= 2.209 kN, M_y= 40.050 & M_{max}= 49.695 kN.mm	1127	12	Spruce	8	380	168	70	90	60	Along grain, DS		11.4	3.33	Decreasing resistance after collapse, with large deformations enhancing ductility. Stiffness was obtained from force–deformation curves.
		1127	12	Chestnut	8	700	168	70	90	60			14.7	5.33	
		1127	12	Spruce CLT	8	420	168	70	90	60			12.6	5.45	
Milch et al. [36]	English oak (Quercus robur L.)	718	12	Norway spruce (Picea abies L. Karst.)	8	475	168	72	18	18	Along grain, SS	1.20	2.74	1.74	Ultimate dowel tearing failure
		718	16		8	487	224	96	24	24		2.02	4.63	2.15	
		718	20		7	503	280	120	30	30		3.30	7.45	2.33	
		718	24		7	473	336	144	36	36		4.40	8.92	2.93	
Zhang et al. [23]	Beech	668	30	Pinus sylvestris	3	504	600	105	175	175	Along grain, DS	25.75	48.52	8.09	No prestress
	Beech	668	30	Pinus sylvestris	3	504	600	105	175	175	(The increased capacity and stiffness in the central two rows is due to prestressing).	36.34	66.34	19.32	10 kN prestress
	Beech	668	30	Pinus sylvestris	3	504	600	105	175	175		42.61	74.31	18.3	20 kN prestress
	Beech	668	30	Spruce	3	446	600	105	175	175		26.46	50.18	8.22	No prestress
Riggio et al. [37]	Beech densified	1170	Square 3 × 3	Spruce	10	390	70	50	25	25	Along grain, SS	-	0.59	0.55	The joint fails either by shear of the peg or by plastic hinge formation.
Khan et al. [26]	Tasmanian Oak	630	19	Radiata pine	5	521	175	45	45		Along grain, DS	5.76	5.94	6.84	Mode V (combined dowel shear and bending with embedment at the dowel-timber interface)
				Side members: Spotted gum Middle: Radiata pine	5	1040/ 521	175	120	42	45		6.52	6.96	6.05	
				Spotted gum	5	1040	175	120	42	42		6.48	6.80	7.11	

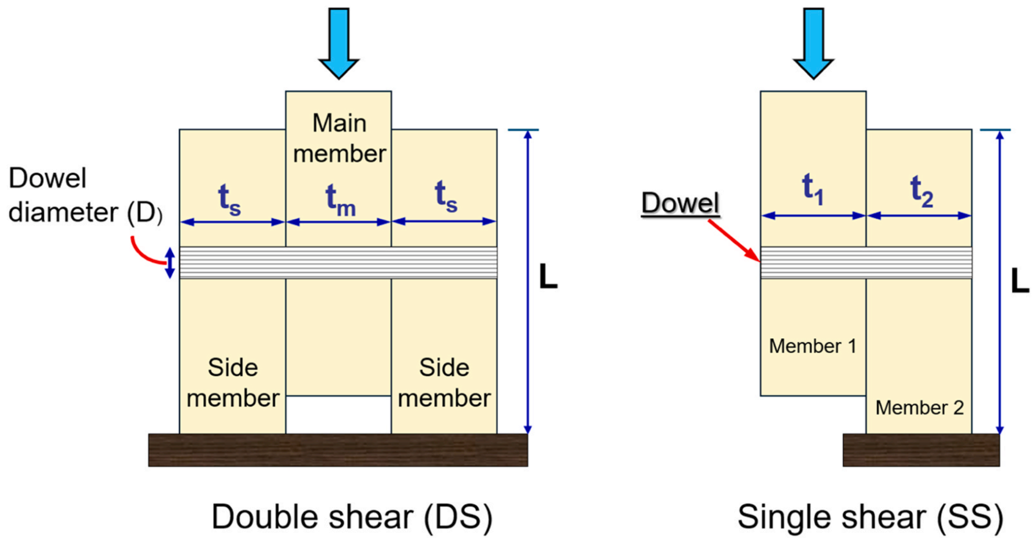

Fig. 1. Single shear (SS) and double shear (DS) connections.

2. Factors affecting the stiffness of WDTC

The factors affecting WDTC performance, as summarized in Table 1, are discussed below.

2.1. Effect of dowel shape

In historical timber structures, wooden fasteners of various shapes were commonly used in joints. Traditional carpentry often employed wooden dowels to secure the relative positions of timber elements. The dowel shape significantly influences the stress distribution beneath it in timber joints. Traetta and Schickhofer [38] reported that a square cross-section dowel, when loaded perpendicular to a flat face, provides higher embedment strength than a circular cross-section, due to a more uniform stress distribution in the timber beneath the dowel. Frontini et al. [21] tested DS connections using round (CYC), octagonal (CYT), and conical dowels (CON, with square and octagonal cross-sections). Their results indicated that octagonal dowels exhibited higher stiffness than round dowels. This increased stiffness was attributed to the tighter fit between the dowel and the hole, which enhances resistance (Frontini et al. [21], Table 1). Nevertheless, additional research is needed to establish more conclusive findings.

2.2. Effect of gaps between members

The failure mode and stiffness of WDTCs are significantly influenced by the spacing between members. Ideally, no gap should exist between the connected members; however, during testing, members can tilt outward, creating a gap, as observed in [18,26,39].

Schmidt and Mackay [40] tested 25.4 mm red oak dowel using the setup in Fig. 2a with shear spans *s* of 6.35, 12.7, and 25.4 mm. The measured joint stiffness decreased with increasing *s*, as shown in Fig. 2b. The original data were reported in imperial units but are converted here to SI for consistency.

Consistent with these trends, Frontini et al. [21] found that SS connections without a gap had higher stiffness than those with a gap (Fig. 3). This effect can be attributed to the fact that the gap introduces additional deformation, creates uneven stress distribution, and alters the failure behaviour, all of which reduce the joint stiffness [23].

2.3. Influence of distances

The end and edge distances required for WDTCs are smaller than those prescribed in the National Design Specifications (NDS) and EC5 for metal fastener connections, owing to the compatibility between wooden dowels and timber that lowers stress concentrations [3]. Burnett et al. [14] used 25.4 mm northern red oak dowels in mortise and tenon joints

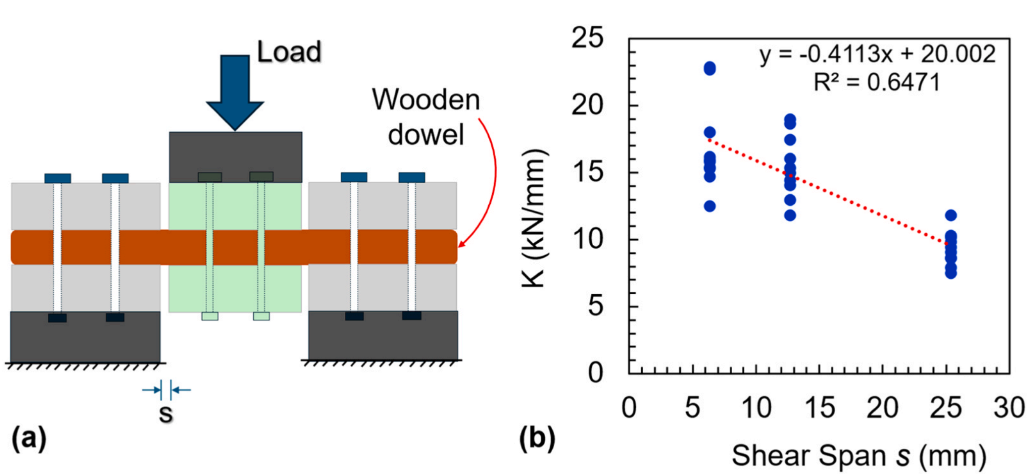

Fig. 2. (a) Shear test setup, where s is the shear span; (b) joint stiffness versus shear span from shear tests [40].

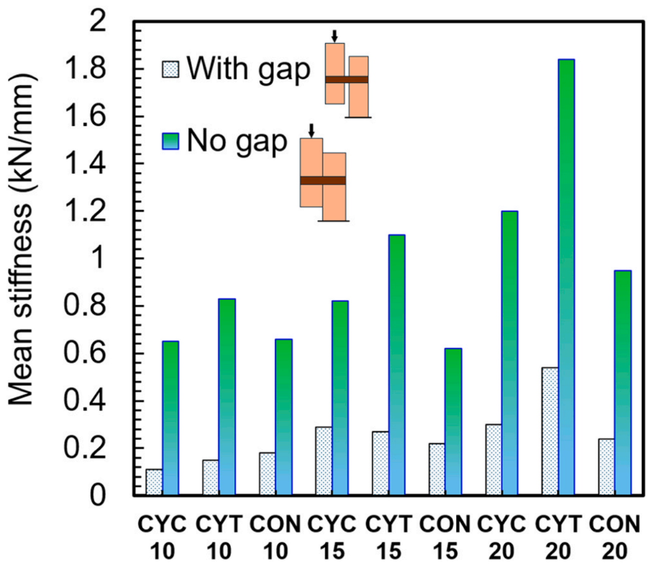

Fig. 3. Joint stiffness K for round (CYC), octagonal (CYT), and conical (CON) dowels with diameters of 10, 15, and 20 mm, tested with and without a gap, using the setup shown in Fig. 2a [21].

of eastern white pine, douglas fir, and northern red oak. They found that end distance had little effect on yield capacity unless reduced to about 50% of the NDS requirement. For eastern white pine, joint stiffness decreased by about 5% when end distance was reduced from 177.8 mm to 25.4 mm; for Douglas fir, stiffness decreased by about 8% when end distance was reduced from 177.8 mm to 58.42 mm. Schmidt and Daniels [41] evaluated WDTCs made from southern yellow pine, Douglas fir, and red oak and recommended minimum distances of 2D for end distance and 2–2.5D for edge distance to ensure ductile behaviour, where D is dowel diameter. Reducing distances below these limits decreased load capacity, whereas increasing them above the minimum gave no further benefit. By comparison, the NDS recommends end distances along the grain for metal fastener connections of 7D for softwood and 5D for hardwood in tension, and 4D in compression, for both loading parallel and perpendicular to the grain, irrespective of timber type. The effect of end and edge distances on stiffness of WDTCs have been studied less extensively and warrants further investigation.

2.4. Direction of testing

ASTM D5652 [30] permits both compressive and tensile loading for connection testing and states that tensile loading is preferred. Along the grain, the elastic modulus is typically higher in tension than in compression by about 5–15%. Tensile loading may therefore produce higher joint stiffness and also avoids potential buckling that can occur in compression. However, for MFTCs the standard requires larger end distances in tension than in compression (seven times the dowel diameter versus four times) [30]. Tensile loading also demands larger member dimensions and can introduce slip at the interfaces when the load is applied. These practical considerations may explain why all studies listed in Table 1 were conducted under compression loading to induce shear in the dowel. Grossi et al. [42] reported no significant difference in shear performance between compression and tension for standard halved and tirolerschloss joints. For WDTCs, where behaviour is largely governed by wooden dowel failure, differences between tensile and compressive loading are expected to be small, but a quantitative assessment is needed to confirm the effect on stiffness.

2.5. Effect of prestress

In WDTC testing, the side members are commonly clamped to prevent lateral opening during loading [26]. However, excessive clamping pressure can influence the stiffness of test results. Zhang et al. [23] investigated DS joints of Pinus sylvestris and spruce with beech dowels under three prestress conditions: none, 10 kN, and 20 kN (Zhang et al. [23], Table 1). The results showed that joint stiffness increased with the application of prestress compared to no prestress. However, increasing prestress from 10 kN to 20 kN produced no significant additional effect. These findings indicate that the presence of prestress enhances joint stiffness but further increases beyond a certain threshold provide negligible improvement. Prestress improves performance by tightening the fit between members, increasing frictional resistance, and promoting a more uniform stress distribution, which collectively enhance the stiffness.

2.6. Effect of dowel specific gravity

Dowel specific gravity is one of the most critical parameters influencing the performance of WDTCs. Vilguts et al. [22] tested CLT SS connections and reported that serviceability stiffness (K_{ser}) are strongly dependent on dowel density. Data presented in Bruzzone et al. [15] and Vilguts et al. [22] further confirm that denser dowels provide greater joint stiffness (Bruzzone et al. [15]; Vilguts et al. [22], Table 1).

2.7. Effect of timber specific gravity

Vilguts et al. [22] tested CLT SS connections and observed that CLT specific gravity has a statistically significant effect on serviceability stiffness (K_{ser}), but no significant effect on yield strength. Data from El Houjeyri et al. [19] (Table 1) indicate that timber density affects both stiffness and strength. Similar trends were observed by Ceraldi et al. [24, 25], Milch et al. [36] and Teodorescu et al. [35], further supporting the influence of timber density on WDTC performance. This effect is quantified in the statistical analysis section.

2.8. Effect of dowel diameter

Vilguts et al. [22] reported that the joint stiffness are directly influenced by dowel diameter. Using two different dowel diameters (19 mm and 25.4 mm) with Douglas Fir, Grand Fir, Western Hemlock, and SPF timber, higher values were observed for the larger dowel diameter, as listed in Table 1 under Vilguts et al. [22]. Additional studies by Frontini et al. [21], Bruzzone et al. [15] and Li and Zhou [20] further support this relationship.

2.9. Influence of member thickness or dowel length

The stiffness of WDTCs is affected by the bearing area. A larger bearing area, or greater member thickness, generally yields higher joint stiffness, consistent with Sandberg et al. [11]. Member thickness also influences failure mode and stress distribution, as discussed in [16], and this is illustrated schematically in Fig. 4. Fukuyama et al. [16] further reported that dowel slenderness, expressed as the length to diameter ratio L/d, affects joint stiffness. This effect is quantified in the *5.1* and *5.2* sections.

3. Assessment of existing empirical models

Failure information for WDTCs is presented in the rightmost columns of Table 1. In most studies, failure occurs as a mixed mode comprising dowel bending, dowel shear, dowel embedment, and timber embedment. This mixed mode is illustrated in Fig. 5. However, this mechanism corresponds to the ultimate failure stage. In contrast, stiffness is determined within the linear elastic range, prior to dowel failure, and reflects the combined contribution of these deformation mechanisms. The following sections critically review and assess existing empirical models, develop new stiffness model using the dataset presented in Table 1, and

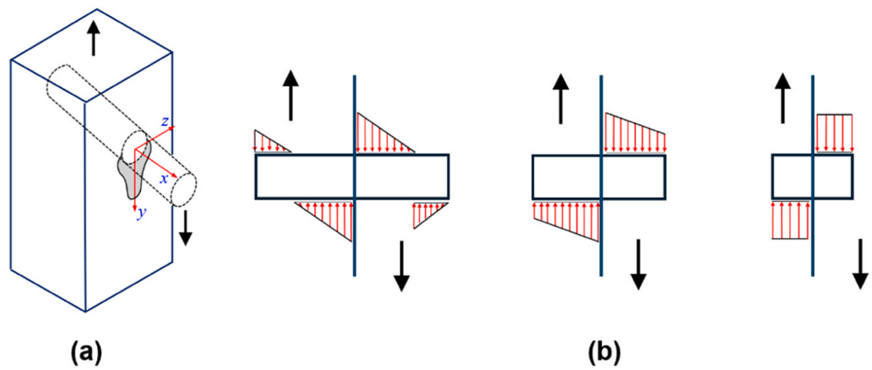

Fig. 4. (a) Bearing stress distribution; (b) Variation of stress distribution with dowel slenderness [16].

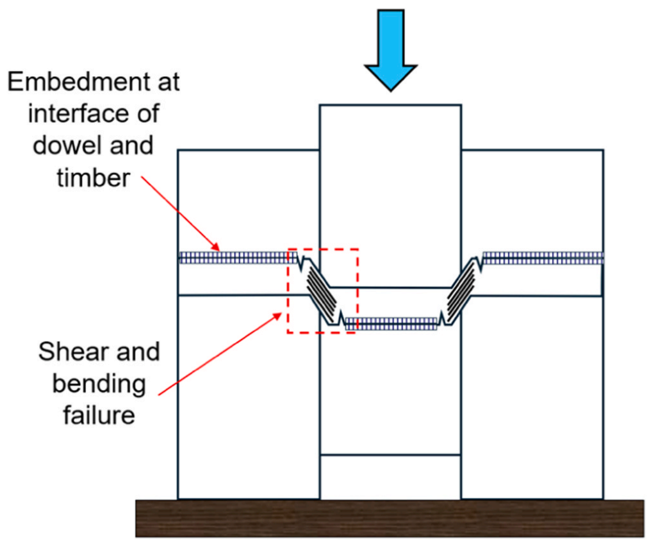

Fig. 5. Typical Mode V failure in WDTCs involving dowel shear, bending, and embedment with minimal timber embedment.

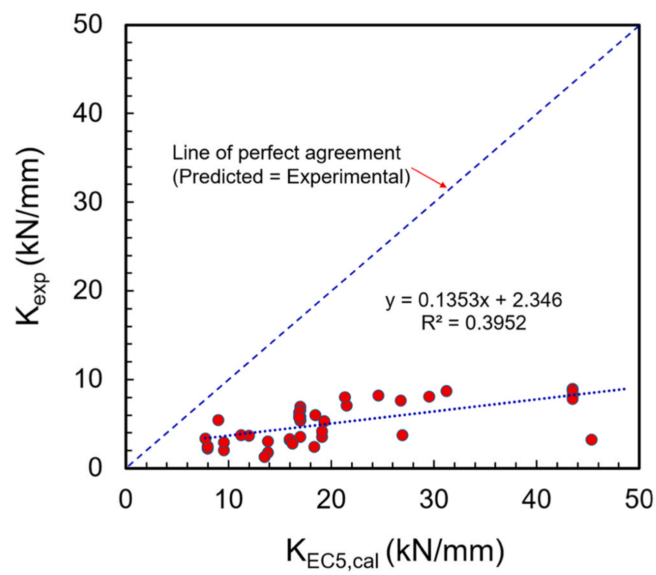

Fig. 6. Comparison of experimental stiffness with Eurocode 5 predictions (Eq. 2).

discuss the sources of deviation in the model predictions. These empirical formulations inherently account for shear and bending effects at the shear plane, as well as embedment at the dowel–timber interface, since they are derived from experimental observations. The existing models are discussed below.

3.1. Eurocode 5

In Eurocode 5, for metal dowels, the slip modulus K_{ser} per shear plane and per fastener is given by Eq. 2, where ρ_m is the mean density of the member material. Predictions from Eq. 2 are plotted against the experimental stiffness (K_{exp}) values listed in Table 1 in Fig. 6. The equation consistently overestimates stiffness across all data points. This bias arises because the formulation neglects dowel deformation and treats the fastener as effectively rigid, an assumption that is inappropriate for WDTCs where both the dowel and the surrounding timber contribute to joint compliance. Applying a reduction factor of 0.22 to Eq. 2 yields a mean $K_{EC5,cal}/K_{exp}$ ratio of 0.89 with a standard deviation (SD) of 0.41.

$$K_{ser} = \frac{\rho_m^{1.5} D}{23} \quad (2)$$

3.2. Joint stiffness model by Vilguts et al

Vilguts et al. [22] tested CLT SS connections and reported that joint stiffness is strongly influenced by dowel specific gravity (G_d), with additional contribution from timber density (G_{CLT}) and dowel diameter. Their regression model is given in Eq. 3.

$$K_{Vilguts,cal} = 0.7 G_d^{2.7} G_{CLT}^{0.25} D \quad R^2 = 0.80 \quad (3)$$

Predictions from Eq. 3 are plotted against the experimental stiffness values in Table 1 in Fig. 7. The ideal prediction places data on the dashed line $y = x$, where experimental and calculated values are equal. The lines 0.75, 0.85, 1.15, and 1.25 represent the ratio of calculated to experimental joint stiffness (K_{cal}/K_{exp}) and show deviation from the ideal $y = x$ line. Data on the 0.75 and 0.85 lines indicate underestimation by 25% and 15%, respectively, whereas data on the 1.15 and 1.25 lines indicate overestimation by 15% and 25%, respectively. The same interpretation of these boundary lines applies to the corresponding figures presented in the subsequent sections.

The model both underestimates and overestimates stiffness, and only a few data points fall between the 0.75 and 1.25 bounds. The dataset exhibits vertical clustering, indicating the presence of influential parameters not included in the model. Cluster 1 corresponds to the results of Frontini et al. [21], who varied dowel cross section shape; this parameter is not represented in the Vilguts et al. model and leads to a vertical strip of points. Cluster 2 also reflects the Frontini et al. [21] series with the same shape effect but with a dowel diameter of 20 mm. Cluster 3 corresponds to Fu et al. [18], who varied side and main member thicknesses which is not included in the model. Clusters 4 and 5 arise from the tests of Sandberg et al. [11], which likewise involve

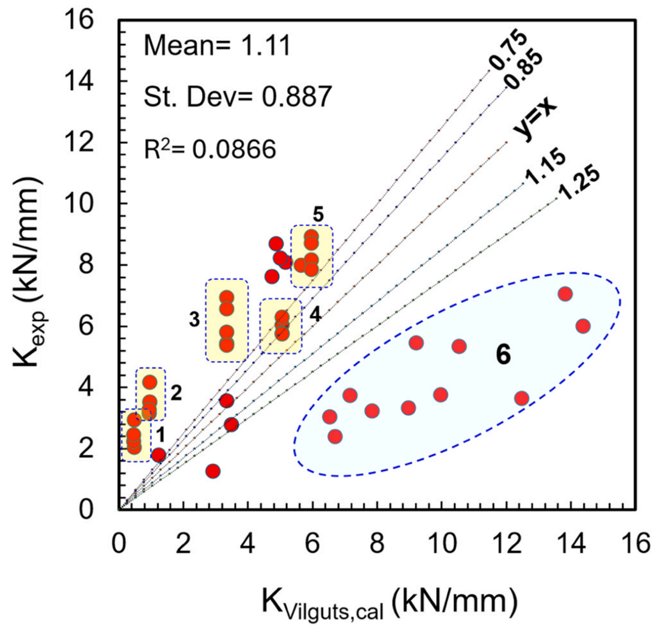

Fig. 7. Comparison of experimental joint stiffness with predictions from the regression model of Vilguts et al. [22].

differences in main member thickness. Since the model was calibrated on CLT with a limited set of species, it does not generalise well to a broader range of species and connection geometries. These observations support the need for models that incorporate geometry and material parameters beyond dowel specific gravity and diameter.

The ratio K_{cal}/K_{exp} has a mean of 1.11, a very high SD of 0.887, and a low correlation (R^2=0.0866). The large SD is driven by the data cluster in region 6. The high predictions in the highlighted Region 6 correspond to datasets from El Houjeyri et al. [19] and Bouhala et al. [33], who used compressed wooden dowels with densities exceeding 1000 kg/m^3 , and from Teodorescu et al. [35], who also used dowels above 1000 kg/m^3 . This model already includes dowel specific gravity with an exponent of 2.7. Consequently, for high density dowels the predicted stiffness is disproportionately amplified, which explains the large positive bias observed for compressed dowels. These results indicate that the Vilguts et al. model is not applicable to compressed or otherwise very high-density dowels.

3.3. Joint stiffness model by Müller et al

Müller et al. [43] proposed a simple model (Eq. 4) to predict joint stiffness (N/mm) per wooden dowel per shear plane, derived from linear regression fitting. This model considers only the dowel diameter.

$$K_{\text{Müller,cal}} = 220d \tag{4}$$

The predictions in Fig. 8 exhibit pronounced vertical clustering of data points. This clustering occurs at more data points than in the Vilguts et al. model because the Müller model includes only dowel diameter and omits influential parameters such as timber density, dowel density, and member thickness. The model both overestimates and underestimates stiffness; accordingly, the mean of the calculated to experimental ratios is close to 1, with a SD of 0.522, which is lower than that of Vilguts et al. About half of the points lie outside the 0.75–1.25 bounds, and the correlation between predicted and measured stiffness is low (R^2 = 0.31). These results indicate that diameter alone is insufficient to capture WDTC stiffness, and that additional material and geometric parameters are required for reliable prediction.

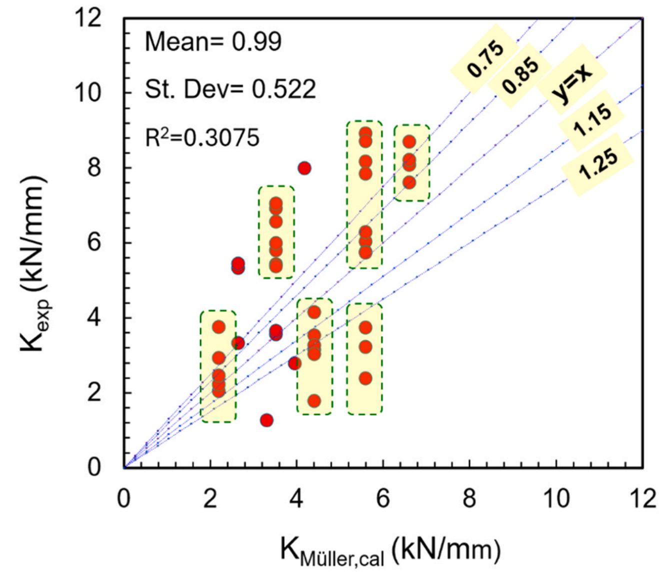

Fig. 8. Comparison of experimental joint stiffness with predicted from Müller et al. proposed equation.

4. Development of a new empirical model

Statistical analyses were conducted to develop a predictive stiffness model for WDTCs using the dataset (644 data points) presented in Table 1. Relevant geometric and material variables reported in Table 1 (ρ_d, D, ρ_t, L, w, t_m, t_s) were initially considered as potential predictors. Efforts were made to maintain a comparable number of data points for each factor to ensure the reliability of the statistical analysis. Subset regression was applied to identify a parsimonious predictor set that achieves optimal predictive performance with the minimum number of input parameters, thereby reducing model complexity and overfitting. Model selection was guided by goodness-of-fit indicators, including the coefficient of determination and prediction error measures. Subsequently, analysis of variance (ANOVA) was performed to quantify the statistical significance and relative contribution of the selected variables to stiffness. This combined approach ensured both predictive efficiency and statistical robustness in the development of the new empirical model. The ANOVA results are listed in Table 2. The overall model, consisting of the variables listed in Table 2, is statistically significant for joint stiffness (F = 34.07, P < 0.001) with R^2 = 0.87, indicating strong explanatory power. As shown in the table, the *P* values for all the variables listed in Table 2 are significantly small, indicating all these variables affects stiffness prediction. Among individual factors, connection length L (F = 58.84) and dowel diameter d (F = 57.22) show the largest effects, followed by timber density ρ_t (F = 39.19), main member thickness t_m (F = 26.06,), and dowel density ρ_d (F = 10.87). These geometric variables are illustrated in Fig. 1. ρ_t is the density of the timber in the

Table 2
ANOVA table for response variable of K.

Source	DF	Adj SS	Adj MS	F-Value	P-Value
Regression	6	155.171	25.8618	34.07	0.000
ρ_d	1	8.251	8.2507	10.87	0.002
D	1	43.43	43.4296	57.22	0.000
ρ_t	1	29.743	29.7428	39.19	0.000
L	1	44.659	44.6587	58.84	0.000
tm	1	19.783	19.783	26.06	0.000
$\rho_t \times \rho_t$	1	25.403	25.4029	33.47	0.000
Error	31	23.529	0.759		
Lack-of-Fit	20	20.22	1.011	3.36	0.021
Pure Error	11	3.309	0.3008		
Total	37	178.7			

WDTC (side and main members). The statistically significant quadratic term ρ_t^2 (F = 33.47) indicates a nonlinear relationship between stiffness and timber density.

From an engineering perspective [16,26], stiffness is governed primarily by geometry and material densities. The member length (L), dowel diameter (d), and member thickness (t_m) influence the bearing area and load transfer path, while material densities control the embedment response. These findings indicate that geometric factors are significant contributors to WDTC stiffness, yet they are often underrepresented in existing theoretical models.

The equation derived from this analysis are presented as Eq. 5 and plotted in Fig. 9. Both equations show high R^2 values, with most predictions falling within the 0.85–1.15 boundary lines. The few data points outside this range are likely due to parameters not included in the model, such as dowel cross-sectional shape and member gaps (Frontini et al. [21]) and prestressing effects (Zhang et al. [23]). The lack-of-fit test is significant (P = 0.021, Table 2), indicating that the current linear model (Eq. 5) does not fully capture all aspects of the stiffness behaviour. Nevertheless, the model demonstrates high predictive accuracy and reliably represents the overall trends observed in the experimental data. It should be noted that this model is based on the averages of 644 data points, and further studies with a broader range of parameters are required to strengthen the regression models.

$$K = -29.04 + 0.002175\rho_d + 0.2483d + 0.1020\rho_t - 0.01064L + 0.02924t_m - 0.000085\rho_t^2 \quad (5)$$

4.1. Embedment modulus: New regression Model

The embedment modulus (k_{emb}) is a key parameter in predicting the joint stiffness of WDTCs, as it serves as an input to both the beam-on-elastic-foundation (BEF) and the rigid rotation with friction (RRF) models, which are discussed in Sections 5.1 and 5.2, respectively. To date, no study has specifically developed a regression model for this parameter. In the present work, embedment testing data with wooden dowels were collected from the literature, including studies by Fu et al. [18], Schmidt and Mackay [40], Church and Tew [44], Ceraldi et al. [24, 25], Guo et al. [45], Zhang et al. [23] and Tomasi et al. [46]. A total of 185 data points were compiled and analysed using ANOVA to identify the parameters influencing the embedment modulus. The parameters dowel specific gravity (G_d), dowel diameter (D), timber specific gravity (G_t), timber member length (L), timber width (w), and member thickness in the dowel embedment direction (t) were considered as potential predictors. A comparable number of data points was maintained for each factor to ensure reliable statistical analysis. The ANOVA results are presented in Table 3, and the resulting model is given in Eq. 6 with units of N/mm^3 .

$$k_{emb} = 69.4 + 0.562t + 10.49G_d - 7.89d + 0.2237d^2 - 0.03131 \quad (6)$$

The ANOVA results demonstrate that the embedment modulus obtained from dowel embedment tests in timber is strongly dependent on specimen's both geometric and material properties. G_d showed the greatest influence (F = 39.19, p < 0.001), confirming that higher-density dowels provide substantially greater stiffness. Timber thickness (t) was also significant (F = 28.41, p < 0.001), indicating that thicker members resist embedment more effectively. Dowel diameter (d) contributed positively (F = 15.68, p < 0.001), while its quadratic term (d^2) was also significant (F = 19.58, p < 0.001), reflecting a nonlinear effect where stiffness does not increase proportionally with size. The interaction between thickness and diameter ($t \times d$) was highly significant (F = 33.65, p < 0.001), suggesting that the effect of dowel diameter is magnified in thicker members. The ranking of factors based on their statistical significance is presented in the rightmost column. Overall, the model accounted for 83% of the variation in embedment modulus (R^2 = 82.98%), with good predictive accuracy (R^2_{pred} = 77.87%). The comparison of experimental and empirically predicted results for embedment modulus (k_{emb}) is presented in Fig. 10. The data from Zhang et al. [23] was used for validation and lies close to the regression line, thereby confirming the model. These quantitative findings confirm that both material density and geometric parameters govern embedment stiffness. The error analysis further supports the robustness of the model. The pure error was very low (MS = 0.4010), showing that replicate tests were consistent and measurement variability was minimal. The lack-of-fit test was not significant at the 5% level (p = 0.061), indicating that the chosen regression model adequately describes the experimental data without systematic deviation.

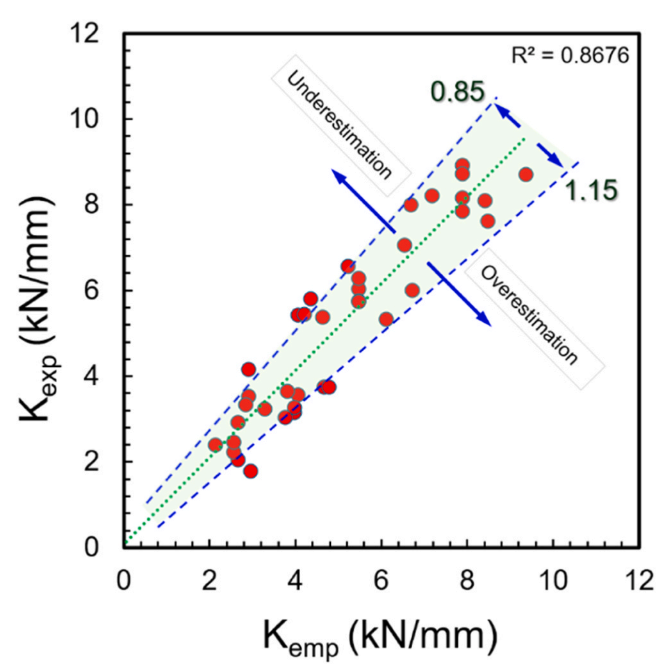

Fig. 9. Comparison of experimental and empirically predicted Joint stiffness K.

Table 3
Results of ANOVA for the response variable k_{emb}.

Source	DF	Adj SS	Adj MS	F-Value	P-Value	Rank
Regression	5	356.75	71.35	38.02	0.000	
t	1	53.31	53.31	28.41	0.000	3
G_d	1	73.54	73.54	39.19	0.000	1
d	1	29.42	29.42	15.68	0.000	5
$d*d$	1	36.75	36.75	19.58	0.000	4
$t*d$	1	63.14	63.14	33.65	0.000	2
Error	39	73.19	1.88			
Lack-of-Fit	35	71.58	2.05	5.10	0.061	
Pure Error	4	1.60	0.40			
Total	44	429.94				

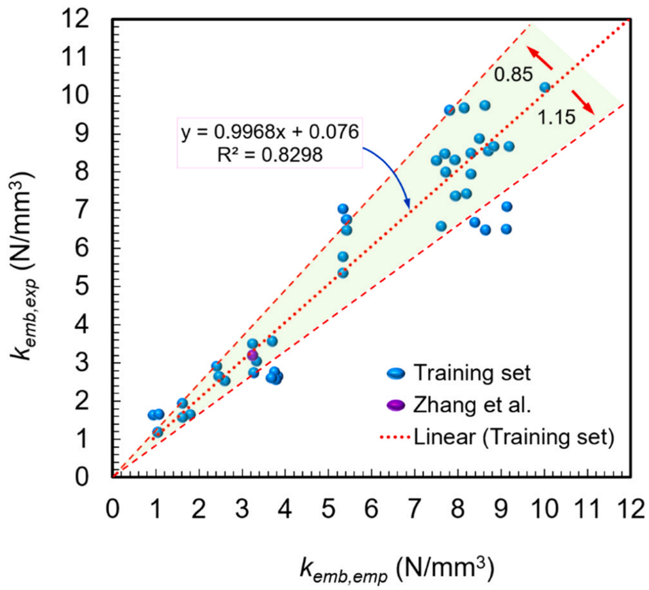

Fig. 10. Comparison of experimental and empirically predicted results for embedment modulus (k_{emb}).

5. Development and assessment of mechanics-based stiffness models

This section presents mechanics-based stiffness models developed to represent the mixed deformation mechanisms governing WDTC behaviour, including dowel bending, dowel shear, dowel embedment, and timber embedment. This mixed-mode response, illustrated in Fig. 5, has been consistently reported in the literature and is summarised in the rightmost columns of Table 1. The dataset compiled in Table 1 is used to critically assess existing formulations, to develop and validate new stiffness models, and to investigate the sources of deviation between predicted and experimental stiffness values.

One of the main novelties of this research is the explicit consideration of shear and bending effects at the shear plane, together with embedment behaviour at the dowel–timber interface. Rather than directly adopting existing formulations, relevant concepts from the literature were carefully examined and further developed into predictive models with explicit attribution. For example, the simply supported beam model was fully derived by the authors while acknowledging its conceptual basis in earlier studies [11]. Similarly, the S-S model and the embedment stiffness–based model proposed herein are, to the authors' knowledge, novel and have not previously been reported for WDTC stiffness prediction.

This study therefore provides not only the formulation of multiple mechanics-based models but also their systematic application and validation against a broad experimental database. In addition, the predictive accuracy and inherent limitations of each model are critically evaluated. The following sections present and discuss the individual mechanics-based stiffness models in detail.

5.1. Joint stiffness based on the Beam-on-Elastic-Foundation

In conventional analysis of dowel-type timber joints, the beam-on-elastic-foundation (BEF) theory is often employed to estimate the initial stiffness of bolted or drift-pin connections. This formulation generally accounts only for bending deformation of the fastener and is expressed in its basic form as Eq. 7:

$$y^{(4)}(x) + \frac{kd}{EI}y(x) = 0 \tag{7}$$

When the fastener is composed of wood or other anisotropic materials, the deformation mechanism differs from that of steel. In such cases, neglecting shear deformation in the analytical model may lead to significant discrepancies between predicted and actual stiffness. To address this limitation, the general beam formulation is extended to include shear deformation effects (Eq. 8) and subsequently simplified into the form shown in Eq. 9. The resulting governing differential equation for the BEF model with shear deformation is then given by Eq. 10.

$$\begin{cases} M(x) = -EI\left(\frac{k'}{GA}w(x) + y''(x)\right) \\ M(x) = EI(u_1 y(x) - y''(x)); w(x) = -kdy(x) \\ Q(x) = \frac{dM(x)}{dx} = EI(u_1 y'(x) - y'''(x)) \end{cases} \tag{8}$$

$$w(x) = -kdy(x) = -EI\left(u_1 y^{(2)}(x) - y^{(4)}(x)\right) \tag{9}$$

$$y^{(4)}(x) - u_1 y^{(2)}(x) + u_2 y(x) = 0 \tag{10}$$

Where $u_1 = \frac{k'kd}{GA}, u_2 = \frac{kd}{EI}$

Here, $k = k_{emb}$ denotes the bearing stiffness [N/mm^3] obtained from dowel embedment in timber; k' is the shear correction factor, defined as the ratio of shear stress at the neutral axis to the average shear stress over the cross-section (k'=4/3 for a circular section [17]); GA is the shear stiffness of the dowel [N]; EI is the bending stiffness of the dowel [N·mm^2]; and d is the dowel diameter [mm].

For shear connections, if the bending moment at the shear plane is assumed to be zero (M=0), as illustrated in Fig. 11a, an exact analytical solution can be derived with relative simplicity [17]. The joint stiffness on one side of the dowel, $K(L)$, is then expressed as a function of the embedment length L according to Eq. 11. This expression is obtained by simplifying Eq. 10 using the boundary condition shown in Fig. 11a; detailed derivations are provided in the study by Fukuyama et al. [17]. For symmetric joints, the embedment lengths in the main and side members are taken as t_m=t_s=L.

$$K(L) = \frac{kd(\alpha^2 + \beta^2 - \alpha^2\cos(2\beta L) - \beta^2\cosh(2\alpha L))}{2\alpha\beta(\alpha\sin(2\beta L) - \beta\sinh(2\alpha L))} \tag{11}$$

Eq. 11 highlights the influence of shear deformation on joint stiffness. Under symmetric boundary conditions with respect to the shear plane (Fig. 11a), it can be rigorously shown that the bending moment at the shear plane is exactly zero. The stiffness–embedment length relationship derived from Eq. 11 is illustrated in Fig. 11b. $K_{ini}(L)$ is the initial slope of $K(L)$ as per Eq. 12. For short embedment lengths, dowel bending and shear deformation are negligible, and the joint response approaches that of an ideally rigid dowel [17]. With increasing embedment length, bending and shear deformation become significant, and the joint stiffness asymptotically approaches a constant value, $K_{Shear+Bending}$. This limiting stiffness is lower than $K_{Bending}$, the value predicted by models that account for bending only (Eq. 13). The trend is plotted in Fig. 11b using data from Zhang et al. [23] for a single dowel, SS connection with E = 15,913 MPa, G= 1056 MPa, k_{emb}= 3.70 N/mm^3, and d= 30 mm. The reduction in stiffness caused by shear deformation can be represented by the reduction factor γ, (γ=$K_{Shear+Bending}/K_{Bending}$). Eq. 14 considers both shear and bending effects. For DS, multiply the result by 2.

$$\lim_{L\to 0} K'(L) = \frac{kd}{4}, \quad K_{ini}(L) = \frac{kd}{4}L \tag{12}$$

$$K_{Bending} = \frac{1}{\sqrt{2}}\left(EI(kd)^3\right)^{\frac{1}{4}} \tag{13}$$

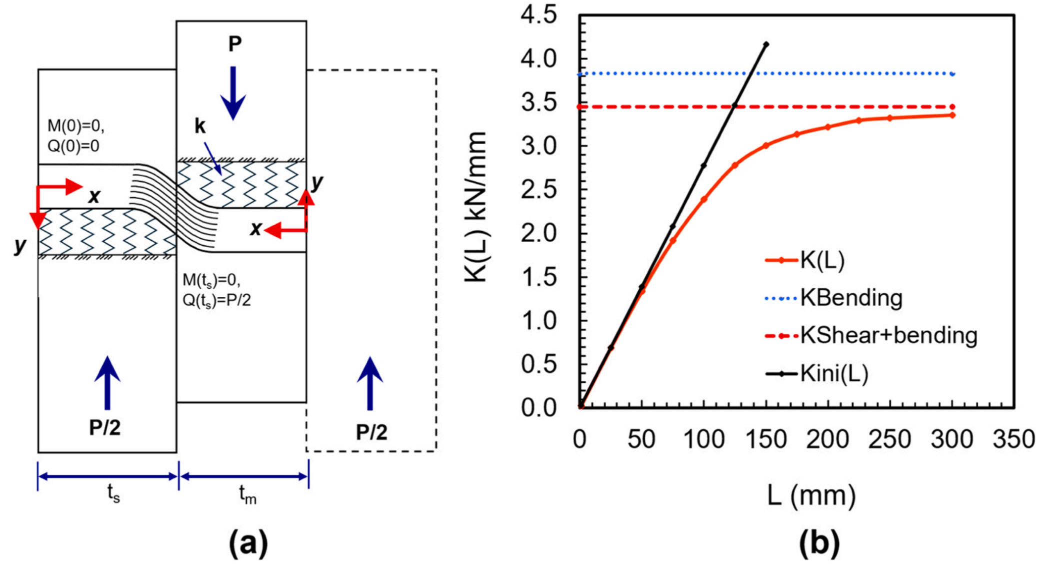

Fig. 11. (a) Boundary conditions of the BEF model; (b) relationship between joint stiffness K(L) and embedment length *L*.

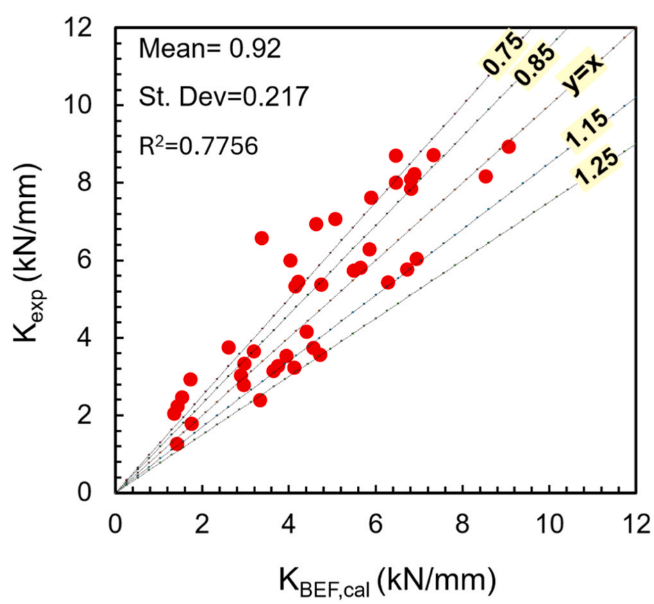

Fig. 12. Comparison of experimental and predicted joint stiffness using the BEF approach.

$$K_{Shear+bending} = K_{BEF,cal} = \frac{1}{\sqrt{2}}\left(EI(kd)^3\right)^{\frac{1}{4}} \times \gamma \quad (14)$$

Where $\gamma^2 = \frac{2\sqrt{u_2}}{u_1+2\sqrt{u_2}} \rightarrow \gamma = \frac{1}{\sqrt{1+\frac{k'}{2GA}\cdot\sqrt{kdEI}}}$

5.1.1. Calculations

To study the general applicability of the BEF model (Eq. 14), the joint stiffness for the data in Table 1 was predicted and plotted in Fig. 12 against the experimental values (K_{exp}). The modulus of elasticity, E, was determined using Eq. 1 for the wooden dowel, while the shear modulus, G, was estimated using the relationship $G=E/16$ as given by EN 384 [28]. The embedment modulus, k_{emb}, was obtained from $k_{emb}=K_{emb}/(dt)$, where K_{emb} is the embedment stiffness, determined either via the S-S approach described in the article [1] or from experimental data reported in the literature by the authors listed in Table 1. For example, Fu et al. and Zhang et al. provide K_{emb} values in addition to their WDTC data. For all data points in Fig. 12, the average ratio $K_{BEF,cal}/K_{exp}$ is 0.92, indicating a good estimation. The bounds of 0.85 and 1.15 represent a ± 15% difference from the experimental joint stiffness values. A few data points fall outside these boundaries; however, they are on the underestimation side, which is considered safe. One reason for this deviation could be that in some studies [20] bamboo dowels were used, for which the current formulation of E and G may not be strictly applicable.

The advantage of this mechanics-based model is that it accounts for the effects of all relevant variables, with an R^2 of 0.78 between experimental and numerical results. This likely explains the absence of vertical strips or clusters in the data. Ideally, the relationship between experimental and calculated values would follow $y = x$. The mean ratio of 0.92 indicates the model underestimates joint stiffness by about 8% on average.

5.2. Joint stiffness based on the Rigid Rotation with Friction (RRF) model

In the BEF model, friction at the dowel–timber interface is ignored, as reported by Fukuyama et al. [16]. In practice, when a wooden dowel is embedded in a timber hole, friction develops at the interface, resisting dowel rotation under load. This resistance generates a restraining moment that reduces or delays rotation [16]. Standard BEF theory does not account for this effect, leading to underestimation of joint stiffness, particularly for short, thick dowels where rotation is significant. Assuming negligible bending and shear deformation in the fastener, rotation angles remain consistent in both Member 1 and Member 2. With friction incorporated, the forces on the fastener resolve as shown in Fig. 13a. This figure is adapted from Fukuyama et al. [16]. Using the coordinate system in Fig. 13b, the resulting bearing strains and stresses distribute as illustrated in Fig. 13c due to equal fastener rotation angles across materials.

Force equilibrium for Material 1 and Material 2 yields Eqs. 15 and 16. Including moment equilibrium about Point O (Fig. 13) with friction effects gives Eq. 17. The Rigid Rotation with Friction (RRF) theory establishes a stiffness model that accounts for friction-inhibited rigid-body rotation. As the slenderness ratio decreases, rotation resistance increases, shifting deformation modes as shown in Fig. 4b. When $r = 0$, pure embedment deformation occurs without rotation (Fig. 4b). For circular sections, the frictional moment arm varies along the z-axis (Fig. 4a), and embedment stress distribution depends on dowel diameter, making the problem inherently indeterminate. Numerical analysis by Fukuyama et al. [16] considered three different embedment stress

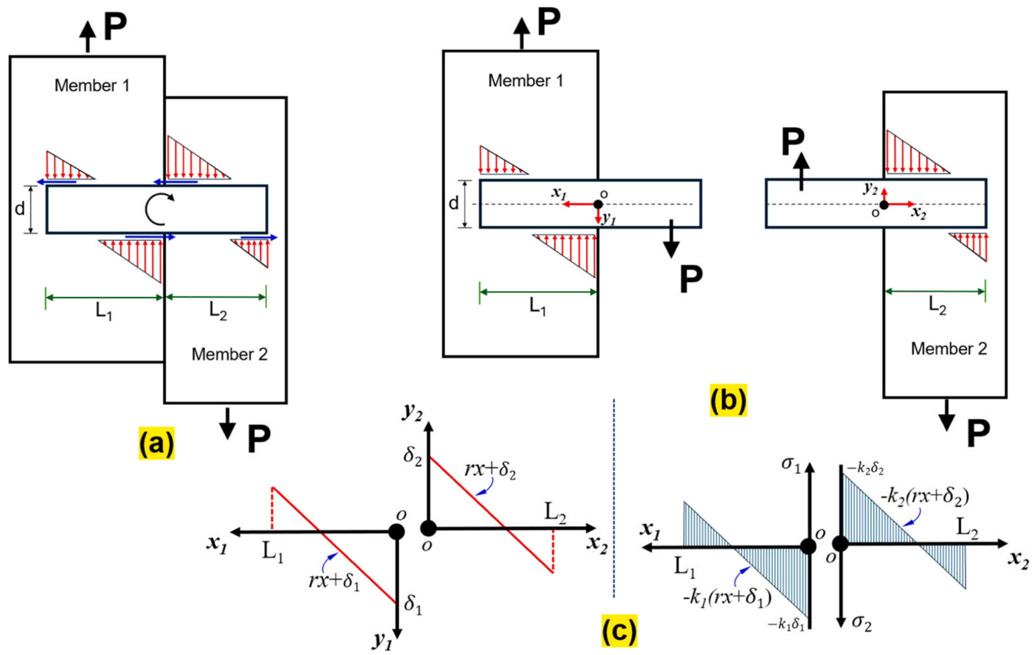

Fig. 13. Short-type SS joint: (a) overall force balance; (b) force balance and distribution in each member; (c) bearing strain and stress distribution [16].

distributions along the y-direction and compared the results with those of a rectangular section of depth *d*. The differences between the assumed patterns were found to be very small. Conservatively, a reduction factor of 0.84 relative to the ellipse section is adopted in this study, due to its close resemblance to a circular section, following Fukuyama et al. [16]. This yields Eq. 17 for circular sections, incorporating the cross-sectional diameter *d*. The BEF model underestimates stiffness at low slenderness ratios by neglecting friction, while the RRF model overestimates stiffness at high slenderness ratios by neglecting shear and bending deformation [16].

$$\int_0^{L_1} k_1 d(rx_1+\delta_1)dx_1 - P = 0 \tag{15}$$

$$\int_0^{L_2} k_2 d(rx_2+\delta_2)dx_2 - P = 0 \tag{16}$$

$$\int_0^{L_1} k_1 d(rx_1+\delta_1)x dx_1 + \int_0^{L_2} k_2 d(rx_2+\delta_2)x dx_2 - 0.84\mu\frac{d^2}{2}.\left(\int_0^{L_1} k_1(rx_1+\delta_1)dx_1 + \int_0^{L_2} k_2(rx_2+\delta_2)dx_2\right) = 0 \tag{17}$$

where: r = rotation angle of the dowel (rad), δ_1= embedment displacement at the interface of material 1 (mm), δ_2 = embedment displacement at the interface of material 2 (mm), k_1= embedment modulus of material 1 (N/mm³), k_2= embedment modulus of material 2 (N/mm³), μ = coefficient of friction between the dowel and the timber hole. By solving Eqs. 15 and 16 for δ_1 and δ_2 and substituting these into Eq. 17, the dowel rotation *r* can be determined. Solving these equations further yields Eq. 18. For symmetric joints, where L_1=L_2=L and k_1=k_2=k = k_{emb}, and defining λ=*L*/*d*, Eq. 18 simplifies to Eq. 19 for a given friction value. In most timber dowel connections, the condition λ> 0.84μ is generally satisfied [16]. For DS, Eq. 19 must be doubled.

$$K = \frac{1}{(\delta_1+\delta_2)} = d\left[\frac{1}{k_1L_1}+\frac{1}{k_2L_2}+\frac{3(L_1+L_2)^2-5.04\mu d(L_1+L_2)}{k_1L_1^3+k_2L_2^3}\right]^{-1} \tag{18}$$

$$K_{RRF,cal} = \begin{cases} \dfrac{kd^2\lambda^2}{8\lambda-5.04\mu}; \lambda > 0.84\mu \\ \dfrac{kd^2\lambda^2}{2}; \lambda \le 0.84\mu \end{cases} \tag{19}$$

If the stress distribution in Fig. 4a is assumed to be square or triangular, with coefficients 0.76 and 0.91 as given by Fukuyama et al. [16], Eqs. 20 and 21 are obtained; further simplification for symmetric joints yields Eqs. 22 and 23, respectively.

$$K = \frac{1}{(\delta_1+\delta_2)} = d\left[\frac{1}{k_1L_1}+\frac{1}{k_2L_2}+\frac{3(L_1+L_2)^2-4.56\mu d(L_1+L_2)}{k_1L_1^3+k_2L_2^3}\right]^{-1} \tag{20}$$

$$K = \frac{1}{(\delta_1+\delta_2)} = d\left[\frac{1}{k_1L_1}+\frac{1}{k_2L_2}+\frac{3(L_1+L_2)^2-5.46\mu d(L_1+L_2)}{k_1L_1^3+k_2L_2^3}\right]^{-1} \tag{21}$$

$$K_{RRF,cal} = \begin{cases} \dfrac{kd^2\lambda^2}{8\lambda-4.56\mu}; \lambda > 0.76\mu \\ \dfrac{kd^2\lambda^2}{2}; \lambda \le 0.76\mu \end{cases} \tag{22}$$

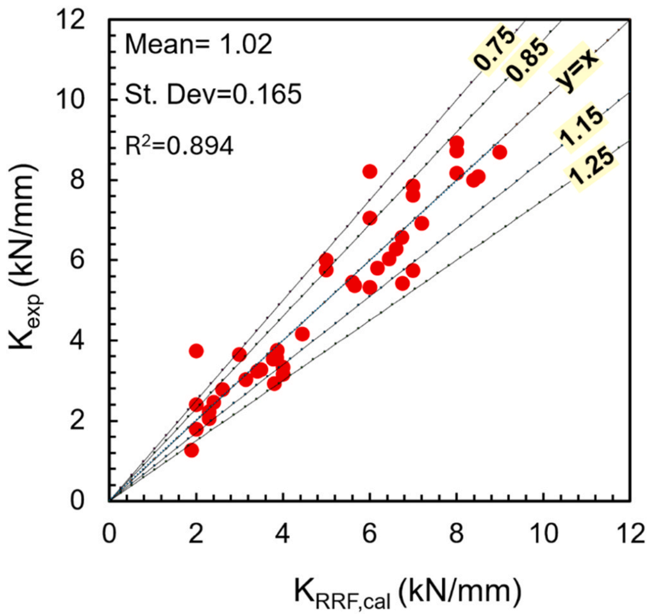

Fig. 14. Comparison of experimental and predicted joint stiffness using the RRF model.

$$K_{RRF,cal} = \begin{cases} \dfrac{kd^2\lambda^2}{8\lambda - 5.46\mu}; \lambda > 0.91\mu \\ \dfrac{kd^2\lambda^2}{2}; \lambda \leq 0.91\mu \end{cases} \quad (23)$$

5.2.1. Calculations

Examining Eqs. 19, 22, and 23 shows only marginal differences in their formulations; therefore, Eq. 19 is adopted in this study. The RRF predictions (Eq. 19) are compared with the data in Table 1 and plotted in Fig. 14. The RRF model provides accurate predictions of joint stiffness. Here, λ represents the ratio of dowel length to its diameter. The embedment modulus, k_{emb}, is determined from $k_{emb}=K_{emb}/(bh)$, where K_{emb} is the embedment stiffness obtained from experimental embedment tests. This model accounts for deformation in both the dowel and the timber substrate through the embedment modulus and also incorporates the effect of friction at the dowel–timber interface. For wood–wood connections, the static friction coefficient μ in drilled holes is taken as 0.6, consistent with literature [47]. The RRF model predicts joint stiffness with high accuracy, with nearly all predicted values differing by less than 25% from the experimental results. Some data points are slightly overestimated or underestimated, likely due to parameters not accounted for in the model. The slightly higher stiffness compared to the BEF model arises from friction, which restrains dowel rotation and enhances stiffness. Overall, for all data points the ratio K_{cal}/K_{exp} has a mean of 1.02, a SD of 0.165, and R^2= 0.894, indicating good predictability.

5.3. Joint stiffness prediction from embedment testing

A new model is proposed to predict WDTC stiffness from embedment tests. Careful examination of previous studies [7,18,23,26] shows that the first deformation observed in WDTCs testing is dowel embedment, followed by other failure modes such as dowel shear, bending, and timber embedment. This sequence is logical, as dowels are loaded perpendicular to the grain, making them highly susceptible to compression. This holds when timber is loaded parallel to the grain.

During dowel embedment, the confinement provided by the notched surrounding timber causes the dowel to partially densify under continued loading, with the load subsequently transferred to the shear plane. At the shear plane, the dowel eventually fails in a mixed mode of shear, bending, and/or timber embedment, commonly referred to as Mode V (Fig. 5). Since stiffness is determined within the initial elastic range, it is reasonable to expect that the stiffness obtained from wooden dowel–timber embedment tests should be slightly higher than that derived from WDTC shear tests. The slightly lower stiffness of WDTCs (15–20%) arises from shear and bending deformations in the elastic range, which are not captured in embedment tests. A brief version of this model was presented by the authors in their recent publication [26]; however, it is developed here in greater detail to provide a more comprehensive explanation. This expanded discussion also facilitates interpretation of the S-S model presented in the following section, as both approaches are founded on the same underlying mechanical concept.

Table 4
Comparison of stiffness from experimental WDTC tests and embedment tests with wooden dowels [26,18,23], (Eq. 24).

References	Dowel Material	Middle & side members	K_{joint} (kN/mm)	K_{emb} (kN/mm)	K_{emb}/K_{joint}	K_{Joint} (kN/mm) (Equation 24)	K_{emb}/K_{joint}
Fu et al. [18]	Beech (Fagus)	Larch LVL	5.43	6.54	1.20	5.56	1.02
			5.80	6.54	1.13	5.56	0.96
			5.37	6.54	1.22	5.56	1.04
			6.93	6.54	0.94	5.56	0.80
			6.57	6.54	1.00	5.56	0.85
Khan et al. [26]	Tasmanian Oak	Spotted gum	7.11	8.82	1.24	7.50	1.05
		Radiata pine	6.84	6.05	0.88	5.14	0.75
Zhang et al. [23]	Beech	Pinus sylvestris	8.09	11.1	1.37	9.44	1.17
	Beech	Spruce	8.22	9.6	1.17	8.16	0.99

To verify this, results from the literature are compared in Table 4. The lower stiffness values from WDTC tests compared to embedment tests are attributed to some deformations at the shear plane, which reduce the measured stiffness. However, the difference is within 15–20%. These findings indicate that joint stiffness, K_{Joint}, is approximately 0.80–0.85 times the embedment stiffness. In Table 4, K_{joint} and K_{emb} are obtained from experimental tests on WDTCs and wooden dowel-timber embedment, respectively. Accordingly, a new model is proposed (Eq. 24) that allows the stiffness of WDTCs to be estimated directly from wooden dowel–timber embedment tests. The rightmost column shows that this model provides improved predictions: values highlighted in light green indicate predictions within 20%, while only one value highlighted in light orange shows a 25% difference. However, only three studies have tested both embedment and connections using the same dowels and member materials (Table 4). Further work is needed to validate and refine the model using experimental data.

$$K_{joint} = 0.85K_{emb} \tag{24}$$

5.4. Joint stiffness predictions using Spring in series approach

A new model is proposed to predict WDTC stiffness using a spring in series (S-S) approach, with the rationale given in *Section 5.3*. This approach is similar to the embedment stiffness-based model in *Section 5.3*, except that stiffness is obtained here from the S-S formulation rather than from direct experimental embedment testing.

The fundamental concept of bearing behaviour is to represent the system as two springs in series (S-S), one corresponding to the bearing stiffness of the base timber and the other to the lateral embedment stiffness of the dowel [1]. This model is expressed mathematically in Eq. 25 and illustrated in Fig. 15d. The factor 0.80 is adopted based on the discussion in *Section 5.3*.

$$K_{S-S,cal} = 0.80 \times \frac{K_t.K_d}{K_t + K_d} \tag{25}$$

where, K_t and K_d are the embedment stiffnesses of the base timber and the dowel, respectively, determined from the test setup shown in Fig. 15. The setup in Fig. 15a follows ASTM D5764–23a [48]. The setup in Fig. 15b is analogous to the ASTM configuration, with the timber member replaced by a steel block and the steel dowel replaced by a wooden dowel. The advantage of this approach is that if K_d and K_t are known, there is no need to perform the test shown in Fig. 15c. The procedure for experimentally determining K_d and K_t is described in the authors' previous studies [1,26]. The wooden dowel–timber embedment stiffness can be obtained using the S-S approach.

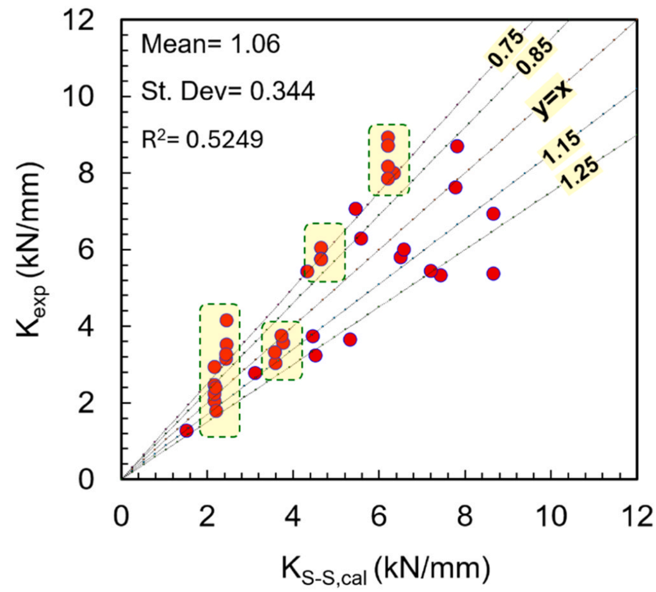

Fig. 16. Comparison of experimental joint stiffness with predictions from S-S approach.

An alternative approach for determining K_t and K_d is to use empirical regression models. Schmidt and Daniels [41] proposed Eq. 26 for K_d based on 30 tests on 25.4 mm white oak dowels, giving stiffness in kN/mm. The value of K_t can be obtained from Eq. 27, adopted from [17], where E_{timber} is in MPa, and t_m and d are in mm; the resulting stiffness is in N/mm.

$$K_d = \quad 28.03G_d^{1.4285}(R^2 = 0.48) \tag{26}$$

$$K_t = \frac{E_{timber}}{31.6 + 10.9d}.dt_m \tag{27}$$

5.4.1. Calculations

Joint stiffness was predicted using Eq. 25 and compared with the experimental results from Table 1 in Fig. 16, showing good agreement in most cases. The timber modulus of elasticity E_{timber} was estimated using Eq. 1. The vertical bands of points in the shaded region indicate that, in some studies listed in Table 1, the side- and main-member thicknesses differed, which influenced joint stiffness but is not captured by the S–S model. In addition, several studies (e.g., Zhang et al. [23], Frontini et al.

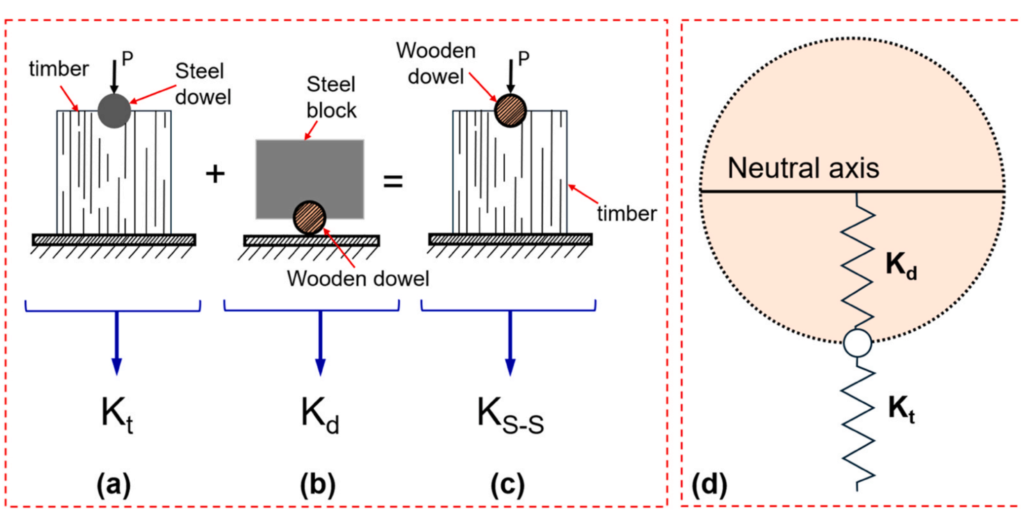

Fig. 15. (a) Steel dowel embedment in timber (b) Wooden dowel embedment under action of steel block (c) Wooden dowel embedment in timber (d) S-S model.

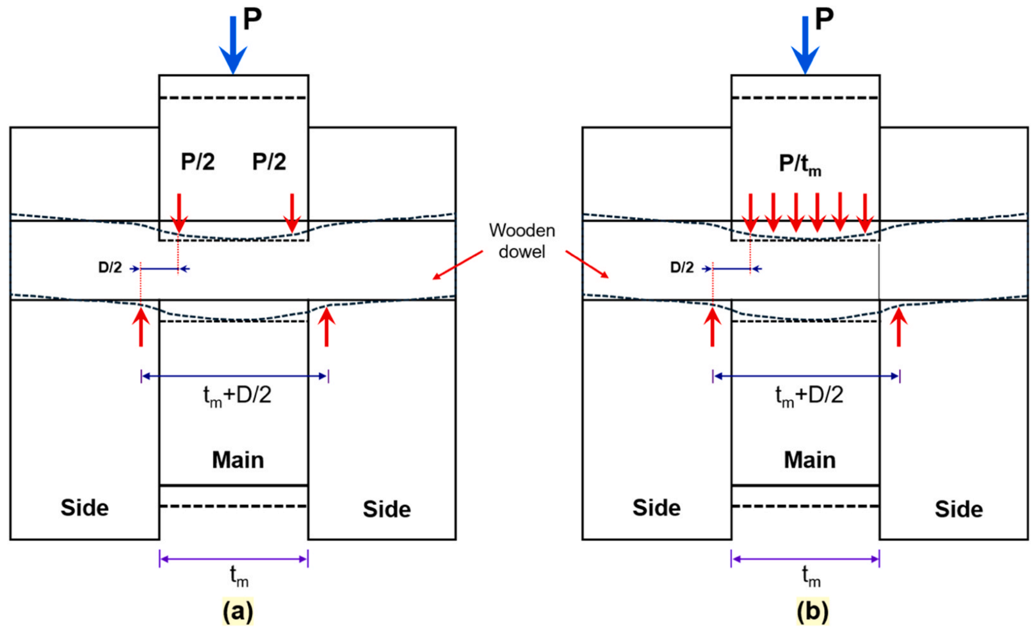

Fig. 17. Dowel stiffness model considering the main member force as (a) a point load and (b) a uniformly distributed load.

[21]) examined member gaps, an effect not included in the present model. Model accuracy could be improved by more precise estimates of K_t and K_d; the current values are obtained from regression. The existing regression model should be improved by incorporating the effects of the governing parameters. The most reliable approach is to determine K_t and K_d directly from experimental embedment tests. Overall, the predictions are good: most data points lie between the 0.75 and 1.25 lines, only a few fall outside, and the mean ratio is about 1.06 with a SD of 0.344.

5.5. Joint stiffness based on post-test deformation of dowel

Careful observation of dowel deformation after testing indicates that the dowel-loading model shown in Fig. 17 is reasonable. The concept of this model was first introduced in reference [11] and is further developed here for WDTCs. In this model, the dowel is treated as a simply supported beam (SSB) subjected to two-point loads (PL), representing the resultant force from the main member, and supported by the side members (Fig. 17a).

To derive the model, concepts from Timoshenko beam theory and elastic bending theory are applied at the shear plane. Both bending and shear deformations are calculated at the shear plane, summed, and converted into a stiffness expression as presented in Eq. 28, thereby incorporating contributions from both bending and shear. The shear modulus is taken as $G=E/16$, following EN 384 [28]. Timber species has a definite effect on local joint deformation, which can be incorporated using the empirical relationship provided in Eq. 29 [11]. The joint stiffness for a DS, single-dowel joint can be approximated using Eq. 30. Here, G_t is the timber specific gravity.

$$K_d = \frac{\pi E_d d}{\left(\frac{4t_m}{d} + 13.733\right)} \tag{28}$$

$$K_t = \frac{1}{-0.169G_{t,oven,dry} + 0.209}\left(kN\Big/mm\right) \tag{29}$$

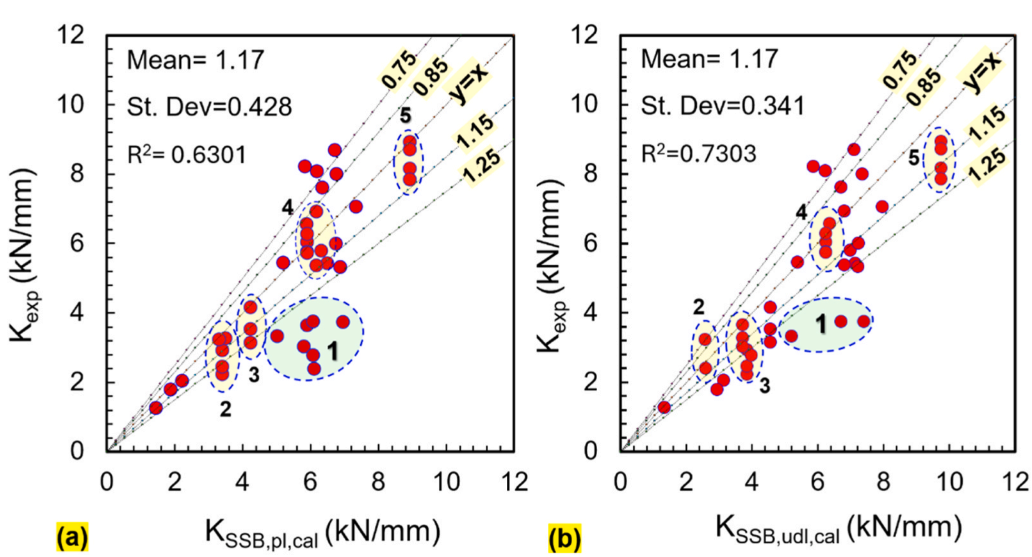

Fig. 18. Comparison of experimental and predicted joint stiffness, considering the main member force as (a) a point load and (b) a uniformly distributed load.

$$K_{SSB,\quad PL,\quad cal} = \frac{K_d K_t}{K_d + K_t} \tag{30}$$

Depending on the dowel slenderness ratio, for dowels with a high slenderness ratio, the load from the main member can be approximated as a uniformly distributed load (UDL) on the dowel (Fig. 17b). The dowel stiffness is then calculated by considering both bending and shear deformations, as expressed in Eq. 31.

$$K_d = \frac{\pi E_d d}{\left(\frac{2t_m^2}{3d^2} + \frac{t_m}{d} + 7.367\right)} \tag{31}$$

5.5.1. Calculations

To apply these models, E_d is estimated using Eq. 1. The models account for both bending and shear deformations of dowels, as well as the thickness of the main member. The results for the point-load and uniformly distributed load models are presented in Fig. 18a and b, respectively. Both variants show a systematic positive bias with mean ratio K_{exp}/K_{cal}= 1.17, indicating overprediction of about 17 %. The UDL assumption performs better overall, giving lower scatter and stronger correlation than the PL case (SD 0.341 vs 0.428; R^2=0.7303 vs 0.6301).

The experimental versus predicted plots reveal vertical clustering (Regions 2–4), where identical model predictions occur despite differing experimental outcomes, indicating that influential parameters are not fully represented. Regions 4 and 5 correspond to Sandberg et al. [11], in which the side member thickness was one half of the main member thickness. Region 3 shows clustered points with small spread and traces to Frontini et al. [21], who tested round, octagonal, and conical dowels of 20 mm diameter; the present model does not include the effect of dowel cross sectional shape. Frontini et al. reported higher stiffness for octagonal dowels than for round dowels, attributable to additional resistance from a tighter fit between dowel and hole. Region 2, also from Frontini et al. [21], involves 10 mm dowels with varying shapes and shows similar clustering.

Region 1 shows overestimation, attributable to use of Sandberg et al.'s expression for timber stiffness K_t, which is valid only for specific gravity in the range 0.40–0.69. Overall, both post-test deformation variants provide reasonable predictions, with a slight bias toward overestimation. Most data lie within the 0.75–1.25 bounds, but the observed clustering underscores the need to incorporate additional geometric and material parameters, including side member thickness and dowel shape, to improve generality.

6. Potential framework for WDTC analysis and design

The proposed formulations for stiffness are presented in Table 5. TFEC 1–2019 is the only standard that provides strength design formulations for mortise and tenon connections using wooden dowels, but it does not include a stiffness model. Joint stiffness is a critical parameter, used as input in the gamma-method and shear analogy method for analysing DLT panels and beams [9,49]. The efficiency of DLT is significantly influenced by joint stiffness [9,50]. For joint stiffness, the minimum value predicted by the models listed in Table 5 should be used.

Table 5
Recommended Models for Predicting Stiffness of Single-Dowel Double-Shear Joints.

K	Models	Remarks
Minimum of	$K_{BEF,cal} = \sqrt{2}(EI(kd)^3)^{\frac{1}{4}} \times \gamma$ $\gamma = \frac{1}{\sqrt{1 + \frac{k'}{2GA}.\sqrt{kdEI}}}$	▪ E from Eq. 1 ▪ G can be estimated using its relationship with E ▪ $k = k_{emb}$ from experimental tests or Eq. 6 or the S-S approach [1]
	$K_{RRF,cal} = \frac{kd^2\lambda^2}{4\lambda - 2.52\mu}; \lambda > 0.84\mu$	▪ $k = k_{emb}$ from experimental tests or Eq. 6 or the S-S approach [1]
	$K_{joint} = 0.85K_{emb}$	▪ K_{emb} from experimental tests ▪ Embedment stiffness (K_{emb}) determined from wooden dowel embedment in timber (Fig. 15c)

These modes require various input parameters such as E, k_{emb}, and G. Currently, no studies provide theoretical models for predicting the embedment modulus k_{emb}, which is used as input in the BEF and RRF models. Developing such models would improve the predictions of RRF, BEF, and SS models. A model has been developed in the present study, as given in Eq. 6, which can be further validated.

The models proposed in this study, based on SSB under point and uniformly distributed loads, may provide improved predictions; however, the timber stiffness K_t used as input is regression-based and derived from a limited dataset. Enhancing the K_t models would further improve prediction accuracy. It has been observed that the thickness of both side and main members affects the stiffness of connections, and this factor should be incorporated into regression models for more accurate results. TFEC recommends that the dowel diameter should not exceed two-thirds of the tenon thickness. One possible approach to account for thickness effects in predictive formulas is to introduce a thickness factor (ratio of the actual thickness of the main/side members to the minimum required thickness). However, further research is needed to establish the minimum thickness requirements for WDTCs.

The embedment modulus k_{emb} must be calculated using the S-S approach. For this purpose, timber should first be tested in embedment using steel dowels as per ASTM D5764 [48]. Wooden dowels should then be tested similarly, replacing the steel dowel with a wooden dowel and the timber block with a semicircular slotted steel block. The embedment modulus from both tests can then be combined using the S-S method to determine the embedment modulus for use in BEF and RRF models [1]. Alternatively, the embedment modulus can be determined directly from tests of wooden dowels in timber; this second method is more direct and accurate but require same timber and dowel properties as used in a DLT.

The scope and applicability of all models presented in the current study depend on the availability of input parameters. For example, the BEF model should be applied when the dowel bending modulus, shear modulus, and the embedment modulus obtained from wooden dowel embedment tests in timber are known. The embedment-based model requires the embedment stiffness of the wooden dowel in timber, while application of the S–S model requires the embedment stiffnesses of both the base timber and the dowel. The RRF model can be used when the embedment modulus and friction at the timber–dowel interface are available. The SSB model is applicable when the dowel bending modulus and timber stiffness are known.

The framework proposed here is intended for use alongside TFEC 1–2019 for single-dowel, shear connections. Dowels should comply with ASTM D8023 [51] requirements, with an oven-dry specific gravity of at least 0.57, be free of defects, and have parallel grain. Factors such as load duration, wet-service conditions, geometry, and temperature should follow the values given in NDS [52] and TFEC [53]. Any factors not covered here can be adopted in accordance with TFEC.

7. Conclusions

In the current study, existing research on wooden dowel-based timber-to-timber connections (WDTCs) was collected and analysed to explore the influence of key parameters on WDTC performance, develop theoretical models for predicting their behaviour, and propose a potential framework for their design and analysis. Key conclusions are as follows:

- The stiffness of WDTCs is influenced by dowel diameter, timber density, dowel density, member sizes, gap between members, dowel shape, and the presence of prestress. End and edge distances affect these parameters minimally when below limiting values but have no influence when above allowable limits based on literature. The most significant parameters are dowel density and diameter; controlling or optimizing these can enhance WDTC performance.

- The BEF, RRF, and embedment-stiffness-based models can be used to estimate joint stiffness. For short, thick dowels, the RRF model governs, while for thin, long dowels, the BEF model is governing. SSB models can also estimate stiffness but require more accurate prediction of timber stiffness. Literature shows that WDTC stiffness ranges from 0.8 to 1.0 times the dowel–timber embedment stiffness (K_{emb}), i.e., K_{joint}= 0.8–1.0K_{emb}. This provides a practical estimate of joint stiffness, potentially reducing the need for additional testing, though it should be validated with larger and more diverse datasets.
- Statistical analyses using best-subsets regression and ANOVA showed that joint stiffness is influenced by ρ_d,D, ρ_t,L,t_m, and $\rho_t.\rho_t$. The thickness of the main member affects stiffness and is an important design factor. A regression model for stiffness was developed based on literature data and is recommended for stiffness prediction. However, its accuracy should be further validated using a broader range of WDTC parameters.
- All theoretical models discussed in this study were validated against a broad range of experimental data. While most models account for WDTC material properties, they often neglect connection geometry, which is also significant. The proposed framework can be used alongside TFEC to estimate WDTC stiffness.

This study is limited to single wooden dowel timber-to-timber connections with loading parallel to the grain. A major strength of this work is its reliance on a comprehensive, consolidated dataset of 644 experimental tests compiled from the existing literature. However, it should be noted that the currently available WDTC data, summarized in Table 1, do not capture all parameters that may influence joint stiffness. Additional factors, such as moisture content of the dowel and timber, surface roughness, dowel geometry, and joint prestress, may affect stiffness but are not considered in the present formulations. These factors require further investigation to evaluate their influence on WDTC stiffness and to develop appropriate modification factors for the equations examined in the present study. The current models do not account for these parameters. The authors encourage future validation and refinement of the proposed models as more WDTC experimental data become available. Multiple-dowel connections are beyond the scope of this study. Although this study is validated using a large, consolidated literature dataset, further validation against fully independent experimental data would enhance the robustness and general applicability of the proposed stiffness models and is recommended for future work.

CRediT authorship contribution statement

Kazem Ghabraie: Writing – review & editing, Supervision. **Mahmud Ashraf:** Supervision, Methodology. **Inayat Ullah Khan:** Writing – original draft, Methodology, Conceptualization. **Mahbube Subhani:** Supervision, Methodology.

Declaration of Competing Interest

The authors declare that they have no known competing financial interests or personal relationships that could have appeared to influence the work reported in this paper.

References

[1] Khan IU, Subhani M, Ghabraie K, Ashraf M. Experimental and empirical study on the embedment behaviour of wooden and steel dowels in hardwood and softwood. Structures 2025;82:110708. https://doi.org/10.1016/j.istruc.2025.110708.
[2] Sotayo A, Bradley D, Bather M, Sareh P, Oudjene M, El-Houjeyri I, et al. Review of state of the art of dowel laminated timber members and densified wood materials as sustainable engineered wood products for construction and building applications. Dev Built Environ 2020;1:100004. https://doi.org/10.1016/j.dibe.2019.100004.
[3] Khan IU, Subhani M, Ghabraie K, Ashraf M. Mechanical performance and design challenges of wooden fasteners: a critical analysis of evaluation methods and standards. Eur J Wood Prod 2025;83:143. https://doi.org/10.1007/s00107-025-02293-1.
[4] Interreg NWE. Towards Adhesive-Free Timber Buildings (AFTB) 2022. ⟨https://vb.nweurope.eu/projects/project-search/towards-adhesive-free-timber-buildings-aftb/⟩ (accessed March 24, 2025).
[5] StructureCraft. Dowel Laminated Timber, The All-Wood Mass Timber Panel. StructureCraft 2024. ⟨https://structurecraft.com/materials/mass-timber/dlt-dowel-laminated-timber⟩ (accessed December 22, 2024).
[6] Khan IU, Subhani M, Ghabraie K, Ashraf M. Exploring and refining testing approaches for hardwood dowels under axial and flexural loading: an experimental and numerical study. Wood Mater Sci Eng 2025;0:1–23. https://doi.org/10.1080/17480272.2025.2505135.
[7] Khan IU, Subhani M, Ghabraie K, Ashraf M. Numerical simulation of wooden dowels under compression. World Conference on Timber Engineering 2025, 2025. Brisbane, Australia: World Conference On Timber Engineering; 2025. p. 2866–73. https://doi.org/10.52202/080513-0350.
[8] Khan IU, Subhani M, Ghabraie K, Ashraf M. Parametric study on the bending performance of wooden dowels. World Conference on Timber Engineering 2025, 2025. Brisbane, Australia: World Conference On Timber Engineering; 2025. p. 2874–80. https://doi.org/10.52202/080513-0351.
[9] Aloisio A, Pasca DP, Tomasi R, Fragiacomo M. Sensitivity of bending stiffness to moisture content in adhesive-free wooden-doweled cross-laminated timber panels. Constr Build Mater 2025;490:142143. https://doi.org/10.1016/j.conbuildmat.2025.142143.
[10] EN 1995-1-1. Eurocode 5: Design of timber structures - Part 1-1: General - Common rules and rules for buildings. Brussels, European Standard: CEN; 2008.
[11] Sandberg LB, Bulleit WM, Reid EH. Strength and Stiffness of Oak Pegs in Traditional Timber-Frame Joints. J Struct Eng 2000;126:717–23. https://doi.org/10.1061/(ASCE)0733-9445(2000)126:6(717).
[12] Khan IU, Subhani M, Ghabraie K, Ashraf M. Novel approaches for shear testing of wooden dowels parallel to the grain: an experimental and numerical study. Eur J Wood Wood Prod 2026. https://doi.org/10.1007/s00107-025-02373-2.
[13] Miller JF, Schmidt RJ, Bulleit WM. New Yield Model for Wood Dowel Connections. J Struct Eng 2010;136:1255–61. https://doi.org/10.1061/(ASCE)ST.1943-541X.0000224.
[14] Burnett DT, Clouston P, Damery DT, Fisette P. Structural properties of pegged timber connections as affected by end distance. Prod J 2003;53:50–7.
[15] Bruzzone G, Godoy D, Quagliotti S, Arrejuría S, Böthig S, Moya L. Experimental Investigation on Dowel Laminated Timber Made of Uruguayan Fast-Grown Species. Forests 2023;14:2215. https://doi.org/10.3390/f14112215.
[16] Fukuyama H, Ando N, Inayama M, Takemura M. Calculation Model and Yield Process of Single Shear Joint with Wood Dowel of Various Slendernesses. J Struct Constr Eng (Trans AIJ) 2008;73:803–10. https://doi.org/10.3130/aijs.73.803.
[17] Fukuyama H, Ando N, Inayama M, Takemura M, Inoue M. Proposal of analytical models of wooden dowel shear joint (in Japanese). J Struct Constr Eng 2007;72:129–36. https://doi.org/10.3130/AIJS.72.129_4.
[18] Fu H, Li Z, Alhaddad W, He M. Experimental evaluation and theoretical prediction of dowel-type joints connecting laminated veneer lumber with wood dowels. Constr Build Mater 2024;416:135248. https://doi.org/10.1016/j.conbuildmat.2024.135248.
[19] El-Houjeyri I, Thi V-D, Oudjene M, Khelifa M, Rogaume Y, Sotayo A, et al. Experimental investigations on adhesive free laminated oak timber beams and timber-to-timber joints assembled using thermo-mechanically compressed wood dowels. Constr Build Mater 2019;222:288–99. https://doi.org/10.1016/j.conbuildmat.2019.05.163.
[20] Li J, Zhou A. Mechanical behavior of laminated bamboo lumber dowel-type connection. Adv Struct Eng 2020;23:65–73. https://doi.org/10.1177/1369433219866091.
[21] Frontini F, Siem J, Renmælmo R. Load-Carrying Capacity and Stiffness of Softwood Wooden Dowel Connections. Int J Archit Herit 2020;14:376–97. https://doi.org/10.1080/15583058.2018.1547798.
[22] Vilguts A, Phillips AR, Jerves R, Antonopoulos C, Griechen D. Monotonic testing of single shear-plane CLT-to-CLT joint with hardwood dowels. J Build Eng 2024;88:109252. https://doi.org/10.1016/j.jobe.2024.109252.
[23] Zhang C, Yang H, Wang Z, Wu M, Shi B, Tao H, et al. Shear characteristics of interfacial timber-to-timber joints for log-wall structures with large-diameter beech dowels: Experimental and theoretical evaluation. Constr Build Mater 2025;458:139536. https://doi.org/10.1016/j.conbuildmat.2024.139536.
[24] Ceraldi C, D'Ambra C, Lippiello M, Prota A. Restoring of timber structures: connections with timber pegs. Eur J Wood Prod 2017;75:957–71. https://doi.org/10.1007/s00107-017-1179-6.
[25] Ceraldi C, Lippiello M, D'ambra C, Prota A. The influence of dowel-bearing strength in designing timber pegged timber joints. Int J Archit Herit 2018;12:362–75. https://doi.org/10.1080/15583058.2017.1323249.
[26] Khan IU, Subhani M, Ghabraie K, Ashraf M. Experimental evaluation and theoretical prediction of single hardwood dowel connections in softwood and hardwood. Eng Struct 2026;353:122251. https://doi.org/10.1016/j.engstruct.2026.122251.
[27] Forest Products Laboratory. Wood handbook: Wood as an engineering material. Madison, WI: U.S. Department of Agriculture, Forest Service, Forest Products Laboratory; 2021.

[28] EN 384 2004. Structural timber — Determination of characteristic values of mechanical properties and density 2004.

[29] ASTM D2395-17 2022. Test Methods for Density and Specific Gravity (Relative Density) of Wood and Wood-Based Materials 2022. https://doi.org/10.1520/D2395-17.

[30] ASTM D5652-21 2021. Test Methods for Single-Bolt Connections in Wood and Wood-Based Products 2021. https://doi.org/10.1520/D5652-21.

[31] ISO/TR 21141 2022. Timber structures — Timber connections and assemblies — Determination of yield and ultimate characteristics and ductility from test data. Switzerland: 2022.

[32] Tétreault M-G, Rollo G, Oudjene M, Fafard M. Experimental investigation on the mechanical characteristics of a novel hybrid densified wood-filled aluminum tube dowel for timber connections. Eng Proc 2023;43:44. https://doi.org/10.3390/engproc2023043044.

[33] Bouhala L, Fiorelli D, Makradi A, Belouettar S, Sotayo A, Bradley D, et al. Advanced numerical investigation on adhesive free timber structures. Compos Struct 2020;246:112389. https://doi.org/10.1016/j.compstruct.2020.112389.

[34] Minari VH, Pereira MCM, Calil Junior C. Adhesive-free structural timber panels: a comparison of stiffness in nail-laminated and dowel-laminated timber panels. Wood Mater Sci Eng 2024:1–11. https://doi.org/10.1080/17480272.2024.2437504.

[35] Teodorescu I, Pereira B, Aquino CD, Branco JM. Experimental evaluation of dowel-type timber joints with wooden dowels. Proc Inst Civil Eng - Struct Build 2020;173:927–38. https://doi.org/10.1680/jstbu.20.00021.

[36] Milch J, Tippner J, Brabec M, Sebera V, Kunecký J, Kloiber M, et al. Experimental testing and theoretical prediction of traditional dowel-type connections in tension parallel to grain. Eng Struct 2017;152:180–7. https://doi.org/10.1016/j.engstruct.2017.08.067.

[37] Riggio M, Sandak J, Sandak A. Densified wooden nails for new timber assemblies and restoration works: A pilot research. Constr Build Mater 2016;102:1084–92. https://doi.org/10.1016/j.conbuildmat.2015.06.045.

[38] Traetta G., Schickhofer G. 2007. Einflussfaktoren auf die Lochleibungsfestigkeit von Fichte und Kiefer für Stabdübelverbindungen. Verbindungstechnik im Ingenieurholzbau, Technische Universität Graz, Hörsaal i12: Verlag der Technischen Universität Graz; 2007..

[39] Vilguts A, Phillips AR, Antonopoulos C, Griechen D. Testing and modeling of CLT-to-CLT joints made using hardwood dowels and screws with varying spacing. Constr Build Mater 2025;458:139449. https://doi.org/10.1016/j.conbuildmat.2024.139449.

[40] Schmidt R, MacKay R. Timber frame tension joinery, 82071. Laramie, WY: Department of Civil and Architectural Engineering University of Wyoming; 1997.

[41] Schmidt RJ, Daniels CE. Design Considerations for Mortise and Tenon. Wyoming Laramie, WY 82071: Department of Civil and Architectural Engineering University of; 1999.

[42] Grossi P, Sartori T, Giongo I, Tomasi R. Analysis of timber log-house construction system via experimental testing and analytical modelling. Constr Build Mater 2016;102:1127–44. https://doi.org/10.1016/j.conbuildmat.2015.10.067.

[43] Müller A, Vogel M, Lang S, Sauser F. Historische Holzverbindungen Untersuchung des Trag- und Lastverformungsverhaltens von historischen Holzverbindungen und Erstellung eines Leitfadens für die Baupraxis. Biel, Switzerland: Bern University of Applied Sciences (BFH) Architecture, Wood, and Civil Engineering Institute for Timber Construction, Structures, and Architecture Competence Area: Building in Existing Contexts and Monument Preservation Solothurnstrasse 102, CH-2504 Biel; 2016.

[44] Church J, Tew B. Bearing Strength of White Oak Pegs in Red Oak and Douglas Fir Timbers. J Test Eval 1998;26:109–14. https://doi.org/10.1520/JTE11980J.

[45] Guo H-F, Xu B-H, Liu X. Experimental analysis of the influence of the fastener material and loaded end and edge distances on the embedment strength parallel to the grain in glued laminated timber. World Conference on Timber Engineering 2025, 2025. Brisbane, Australia: World Conference On Timber Engineering; 2025. p. 4475–80. https://doi.org/10.52202/080513-0551.

[46] Tomasi R, De Santis Y, Aloisio A, Crocetti R, Sæby VH, Nyrud AQ. Experimental and analytical investigation on timber connections with beech, birch and laminated densified wooden dowels. Constr Build Mater 2025;494:142692. https://doi.org/10.1016/j.conbuildmat.2025.142692.

[47] McKenzie WM, Karpovich H. The frictional behaviour of wood. Wood Sci Technol 1968;2:139–52. https://doi.org/10.1007/BF00394962.

[48] ASTM D5764 2023. Standard Test Method for Evaluating Dowel-Bearing Strength of Wood and Wood-Based Products. 2023. https://doi.org/10.1520/D5764-97AR18.

[49] Li X, Ashraf M, Subhani M, Kremer P, Li H, Anwar-Us-Saadat M. Rolling shear properties of cross-laminated timber (CLT) made from Australian Radiata Pine – An experimental study. Structures 2021;33:423–32. https://doi.org/10.1016/j.istruc.2021.04.067.

[50] O'Loinsigh C, Oudjene M, Shotton E, Pizzi A, Fanning P. Mechanical behaviour and 3D stress analysis of multi-layered wooden beams made with welded-through wood dowels. Compos Struct 2012;94:313–21. https://doi.org/10.1016/j.compstruct.2011.08.029.

[51] ASTM D8023-23 2023. Specification for Round Wood Dowels (Pegs) for Use in Wood Construction 2023. https://doi.org/10.1520/D8023-23.

[52] NDS. National Design Specification (NDS) for Wood Construction. Leesburg, VA United States: American Wood Council; 2018.

[53] DeStefano J., Hershberger J., Luthi T., Lynch J., Nehil T., Schmidt D., 2019. Standard for Design of Timber Frame Structures and Commentary 2019.